Quantum dynamics of atoms in number-theory-inspired potentials

D. Cassettari,[1,*] O. V. Marchukov,[2] B. Carruthers,[1] H. Kendell,[3,4] J. Ruhl,[5] B. De Mitchell Pierre,[6] C. Zara,[6] C. A. Weidner,[4] A. Trombettoni,[7,8] M. Olshanii,[5] and G. Mussardo[8]

[1]*SUPA School of Physics and Astronomy, University of St Andrews, North Haugh, St Andrews KY16 9SS, United Kingdom*
[2]*Institute of Photonics, Leibniz University Hannover, Nienburger St. 17, 30167 Hannover, Germany*
[3]*Quantum Engineering Centre for Doctoral Training, University of Bristol, Bristol BS8 1FD, United Kingdom*
[4]*Quantum Engineering Technology Laboratories, H. H. Wills Physics Laboratory and Department of Electrical and Electronic Engineering, University of Bristol, Bristol BS8 1FD, United Kingdom*
[5]*Department of Physics, University of Massachusetts Boston, Boston Massachusetts 02125, USA*
[6]*Department of Mathematics, University of Massachusetts Boston, Boston Massachusetts 02125, USA*
[7]*Department of Physics, University of Trieste, Strada Costiera 11, I-34151 Trieste, Italy*
[8]*SISSA and INFN, Sezione di Trieste, Via Bonomea 265, I-34136 Trieste, Italy*

(Received 12 September 2025; accepted 13 January 2026; published 19 March 2026)

In this paper we study transitions of atoms between energy levels of several number-theory-inspired trapping potentials under the effect of time-dependent perturbations. First, we simulate in detail the case of a trap whose single-particle spectrum is given by the prime numbers. We investigate one-body Rabi oscillations and the excitation line shape for two resonantly coupled energy levels, and we show that quantum control is a faster method for state preparation than periodic perturbation. Next, we investigate cascades of such transitions, particularly whether one can construct a quantum system where the existence of a continuous resonant cascade from a given initial energy eigenstate is predicated by the validity of a given statement in number theory. We find that such resonance cascades, in a suitably designed one-body system, can be used to illustrate that the sequence of natural numbers is closed under multiplication. We further present ideas for two more resonance cascade experiments designed to illustrate certain statements within the Diophantus-Brahmagupta-Fibonacci identity and the Goldbach conjecture.

DOI: 10.1103/cpm3-lpgp

I. INTRODUCTION

In recent years, optical trapping of ultracold atoms has advanced to the point that it is now possible to control, with precision, the profile of the trapping potential. This progress has been enabled by light sculpting techniques [1] relying on the use of spatial light modulators [2], digital micromirror devices [3,4], and fast-scanning acousto-optic deflectors [5].

These developments are particularly suited to address, in a realistic and tunable setup, suggestions and ideas at the interface between quantum physics and number theory [6–8]. To this end there has recently been experimental progress in creating *prime number potentials* for cold atoms [9]. These are trapping potentials whose first N_b eigenenergies are proportional to the first N_b prime numbers. The rationale is that such highly controllable potentials, which can in general be engineered to have an assigned sequence of numbers as their energy levels, are relevant for a host of theoretical ideas. For instance, they can be used for the implementation of primality tests [6], prime factorization of integers (see Refs. [10,11] and references therein), and for studying statements from number theory such as the Goldbach conjecture, which states that every even natural number greater than two can be written as sum of two prime numbers. Of course, one cannot prove mathematical theorems by using a physical device in which a finite (even very large) number of prime numbers is encoded—but, on the other hand, one can systematically extract predictions from number theory theorems and conjectures and design experiments based on them (possibly looking for counterexamples for conjectures). At the same time, by cross-fertilization, the physical realization of number-theory-inspired setups can generate new ideas to tackle number theory problems.

In this paper, we consider one-dimensional trapping potentials where the energy levels of the system have been engineered to produce a desired spectrum, and we study transitions between energy levels under the effect of time-dependent perturbations. We consider two complementary scenarios. First, in Sec. II we study transitions in a potential with energy levels proportional to the first N_b prime numbers. As the prime numbers are not regularly spaced, a time-dependent perturbation on resonance between the ground state and a target excited state transfers population between these states, while the population of other states remains negligible. We also explore how quantum control protocols can speed up this state preparation. We remind that the selective excitation

*Contact author: dc43@st-andrews.ac.uk

of just one state is a critical state preparation step prior to carrying out factorization algorithms described in Refs. [11,12].

The next sections of the paper are dedicated to further exploration of the use of spectrally engineered systems. In Secs. III and IV we introduce *resonance cascades*, where a particle prepared in a given highly excited state is induced to cascade down in energy due to an external perturbation. We use these resonance cascades as a paradigm to study a set of statements from number theory. As a test bench, we consider a potential with an energy spectrum given by the logarithms of the natural numbers. Here we find that, because the sequence of natural numbers is closed under multiplication, a perturbation at an appropriate frequency can generate a resonance cascade (or ladder), in which many levels are populated. Conversely, if we remove from the spectrum the logarithm of one of the natural numbers, then this resonance cascade is inhibited.

Finally, in Sec. V we outline future ideas on how resonance cascades can be used to study the Diophantus-Brahmagupta-Fibonacci identity [13] (Lemma 1, p. 142) and the Goldbach conjecture [13] (p. 147). In the first case, the potential of interest has energy levels given by the logarithm of the sum of two integers squared, whereas the second case is based on the prime number potential investigated in Sec. II, but where a cascade is enabled if the potential contains two weakly interacting particles. Thus, this work outlines and studies in detail the necessary ingredients to test experimentally several number-theoretic statements, from the spectral engineering to the initial state preparation and driving required to demonstrate, via resonance cascades, the identities and conjectures under study.

II. A RESONANCE IN THE PRIME NUMBER POTENTIAL

In this section, we discuss the relevant state preparation required for the subsequent number-theoretic experiments. We explore this in two ways: first through perturbative driving on resonance, where we recover behavior similar to Rabi oscillations between the interrogated states. Second, we explore the potential of quantum control to speed up state preparation, showing that the state transfer can be sped up by about a factor of five.

A. Periodic perturbations

Let us consider the one-dimensional Hamiltonian:

$$\hat{H}^P = \frac{\hat{p}^2}{2m} + U^P(x), \tag{1}$$

where $U^P(x)$ is a potential having as assigned spectrum the first N_b prime numbers times an energy scale, denoted by U_0, depending on the physical realization of the system. To be more precise, we could use the notation $U^P_{N_b}(x)$, but for the sake of simplicity we will omit the index N_b. The potential $U^P(x)$ is referred to as the *prime number potential*.

Figure 1 shows $U^P(x)$ with eigenvalues given by the first $N_b = 20$ prime numbers:

$$E^P_n = U_0 p_n$$
$$p_1,\ p_2,\ p_3,\ \ldots p_{20} = 2,\ 3,\ 5,\ 7,\ \ldots 71. \tag{2}$$

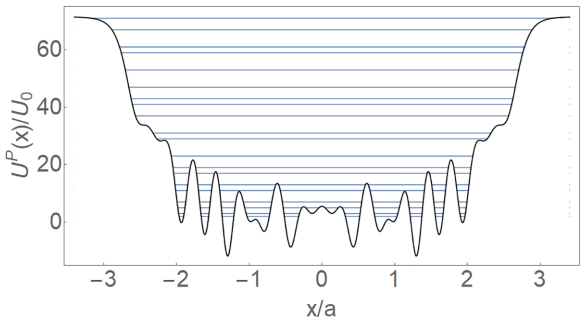

FIG. 1. Prime number potential with 20 energy levels corresponding to the first 20 prime numbers. Here $a = \hbar/\sqrt{mU_0}$ is the characteristic length scale of the potential (with m the particle mass) and U_0 is the corresponding energy scale.

This potential has been calculated using the methods of supersymmetric quantum mechanics and has been optically implemented with a spatial light modulator [9]. In general, the methods used to calculate this potential can be used to calculate potentials with arbitrary (and finite) spectra. Notice that $U^P(x)$ is going to a constant as $x \to \infty$, so that above the eigenvalue p_{20} the continuous part of the spectrum starts. From now on, we measure energies in units of the energy scale U_0 and lengths in units of the quantity $a = \hbar/\sqrt{mU_0}$.

In this section we simulate the transfer between bound states of this prime number potential by applying time-dependent perturbations of the form

$$V(x,t) = f(x)\cos(\omega t), \tag{3}$$

where we examine two cases for $f(x)$ (see Fig. 2): $f_{\text{odd}}(x) = \beta(x/a)$ and $f_{\text{even}}(x) = \beta(x/a)^2$, which induce transitions between states of opposite parity and between states of the same parity, respectively. Specifically, $f_{\text{odd}}(x)$ enables the transfer between the ground state $|0\rangle$ and the first-excited state $|1\rangle$, while $f_{\text{even}}(x)$ enables the transfer between $|0\rangle$ and the second-excited state $|2\rangle$. In both cases, the perturbation is close to resonance with the transition ($\omega = U_0/\hbar$ and $\omega = 3U_0/\hbar$ for the first and second excited states, respectively), and the anharmonicity of the potential ensures that the population of higher states remains small, so that we have essentially isolated a two-level system. Experimentally, these perturbations can be realized with additional optical or magnetic fields. Figure 3 shows Rabi oscillations between $|0\rangle$ and $|1\rangle$ (a) and between $|0\rangle$ and the $|2\rangle$ (b), both obtained by numerical integration of the time-dependent Schrödinger equation. The

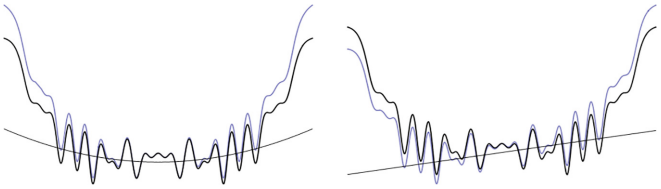

FIG. 2. Even (left) and odd (right) perturbations, where $\beta = 2$ for the even case and $\beta = 4$ for the odd case. These values of β are significantly larger than those used in the simulations to better visualize the effect of the perturbations on the potential. The axes on these plots are the same as in Fig. 1.

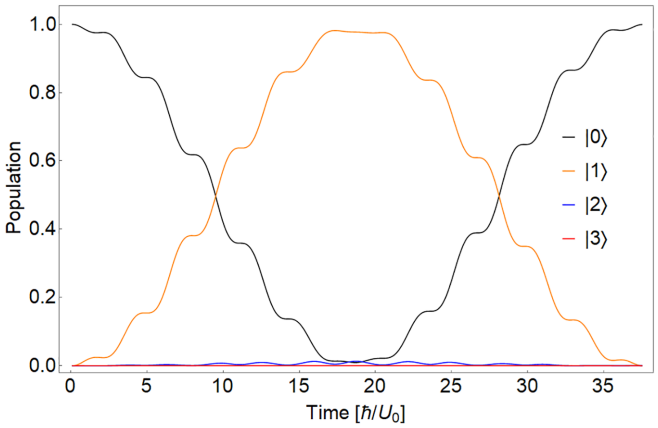

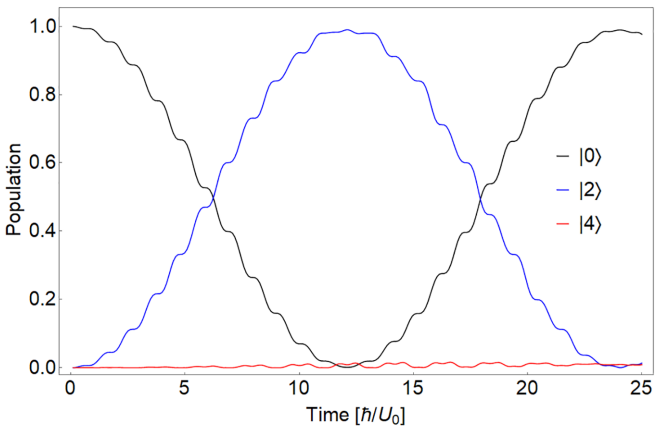

FIG. 3. (a) Odd transition between the ground state and first excited state with $\beta = 0.25$, where a small population of the second excited state can be seen. (b) Even transition between the ground state and second excited state with $\beta = 0.5$. This driving strength also leads to a small but visible population of the fourth excited state (the next transition of even parity).

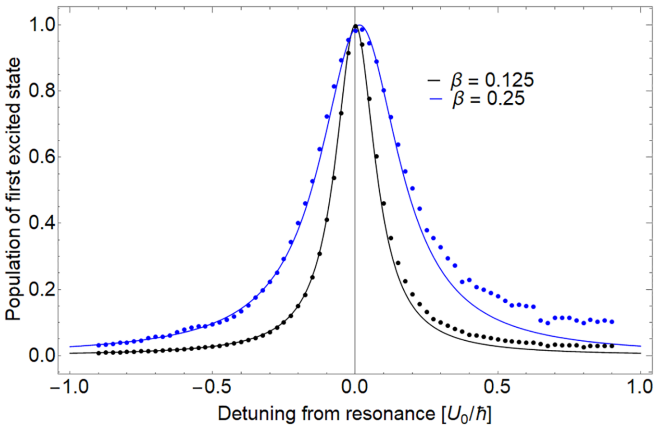

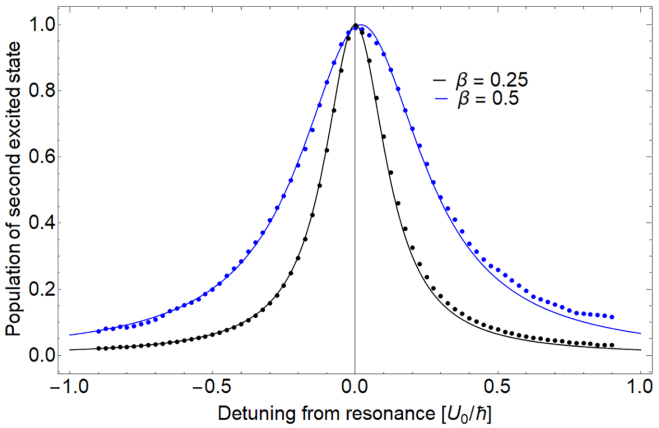

FIG. 4. (a) Line shape of the odd transition for $\beta = 0.125$ and $\beta = 0.25$. (b) Line shape of the even transition for $\beta = 0.25$ and $\beta = 0.5$. Numerical data are displayed alongside Eq. (4) with their respective value of Ω_R. We note that for the same value $\beta = 0.25$, the width of the odd transition is larger than the width of the even transition. This is due to the different couplings, as $\langle 0|x|1\rangle = 0.68$ and $\langle 0|x^2|2\rangle = 0.52$.

Rabi frequency Ω_R is given by the matrix element of the perturbation between the ground state and the desired excited state [14]. The β values are chosen according to the following criterion: A larger β would lead to a higher Rabi frequency and a faster transfer to the desired excited state, which is experimentally advantageous; however, this would come at the price of reduced efficiency of the transfer to the desired excited state, because a larger β would increase the population of higher states. In this respect, Fig. 3 shows the fastest possible transfer while achieving a good fidelity corresponding to $>98\%$ of the population in the desired excited state. Note that in addition to the Rabi oscillations, the time evolution also displays fast ripples at frequency 2ω. These are due to the fact that the rotating-wave approximation is not perfectly satisfied for the perturbation strengths we are using.

To further characterize the system, we study the effect of off-resonant perturbations. For a two-level system in the rotating-wave approximation, the maximum population of the excited state is

$$P_{\mathrm{ex,max}} = \frac{\Omega_R^2}{\Omega_R^2 + \delta^2}, \tag{4}$$

where δ is the detuning from resonance [14]. The maximum population is 1 for resonant perturbation ($\delta = 0$) and displays a Lorentzian line shape for finite detunings with FWHM $= 2\Omega_R$. These Lorentzian line shapes are found numerically in our system for both the odd and the even transition, as shown in Fig. 4. The good agreement between the numerical data and Eq. (4) (with the value of Ω_R calculated from the relevant matrix element of the perturbation) shows that our system behaves as a two-level system to a good approximation. We note that for larger values of β, the center of the transition slightly shifts to the right. We attribute this to the Bloch-Siegert effect [15], which occurs beyond the rotating-wave approximation. Similarly, the deviation of the numerical data from the Lorentzian, visible at positive detunings, is also likely due to the rotating-wave approximation not being well satisfied.

In an experimental implementation with ultracold atoms (for instance, in rubidium), the typical resonance frequencies will be $\sim$1 Hz and typical transfer times to the excited state will be on the order of 10 s. These slow timescales

TABLE I. Optimized transfer times ($\mathcal{F} > 0.99$) from the ground state for a variety of protocols. Note that the case shown as $\gg 12\,\hbar/U_0$ has not been optimized for longer times due to computer cluster limitations.

Transfer time ($\hbar/U_0$)	$\|1\rangle$	$\|2\rangle$	$\|3\rangle$
$\beta = 0.5, n = 2$	–	9.5	–
$\beta = 1, n = 2$	–	5.0	–
$\beta = 2, n = 2$	–	3.0	–
$\beta = 10, n = 2$	–	2.0	–
$\beta = 0.5, n = 1$	7.5	–	$\gg 12.0$
$\beta = 1, n = 1$	5.5	–	9.0
$\beta = 2, n = 1$	4.0	–	7.0

are because the characteristic length scale of the potential a needs to be well above the optical resolution of the optical system that produces the potential. This constraint on a puts an upper limit on U_0 via $a = \hbar/\sqrt{mU_0}$ and, consequently, a lower limit on the time unit $\hbar/U_0$ [9]. Higher-resolution projection systems providing smaller a values (as in quantum gas microscopes [16,17]) allows for faster state transfers. However, even with modest values of a, we can speed up state transfer via optimal control methods, as we show next.

B. Quantum control

In this section, we explore two state transfer protocols simulated using the QEngine C++ library [18] and optimized using the GRAPE algorithm [19] implemented within QEngine:

(1) $\beta(x/a)^2$ modulation for $|0\rangle \rightarrow |2\rangle$ transfer,

(2) $\beta(x/a)$ modulation for $|0\rangle \rightarrow |1\rangle$ and $|0\rangle \rightarrow |3\rangle$ transfer.

For each case, we implement a control of the form $\beta\, b(t)(x/a)^n$ with $n = 1, 2$ for the linear and quadratic cases, respectively. The control $b(t)$ is optimized for a given static value of β and $-1 \leqslant b(t) \leqslant 1\,\forall\, t$.

These protocols provide a benchmark that serves to compare optimal control results with resonant driving results, as well as demonstrating an interesting state preparation proof-of-principle that can be useful for, e.g., the resonant cascade protocols described in later sections of the paper. For the optimization, the initial state is the ground state of the prime number potential, and we use regularization [20,21] to limit the bandwidth of the control in order to preserve experimental viability.

Using the unit scalings provided, the best results are tabulated in Table I, and plots of the fidelity vs control time for $\beta(x/a)^2$ and $\beta(x/a)$ are shown in Fig. 5. These show the minimum time required for a control to reach 0.99 fidelity, where fidelity is defined as $\mathcal{F} = |\langle\psi_{\text{des}}|\psi_{\text{opt}}\rangle|^2$, with $|\psi_{\text{des}}\rangle$ corresponding to the either $|1\rangle$, $|2\rangle$, or $|3\rangle$ and $|\psi_{\text{opt}}\rangle$ the final state after optimization. The infidelity is $\mathcal{I} = 1 - \mathcal{F}$. The optimal controls (i.e., those found at the minimum time where $\mathcal{F} > 0.99$) are plotted in Fig. 6 for $\beta = 0.5$.

The results in Table I show that quantum control enables the transfer to the desired excited state with fidelities

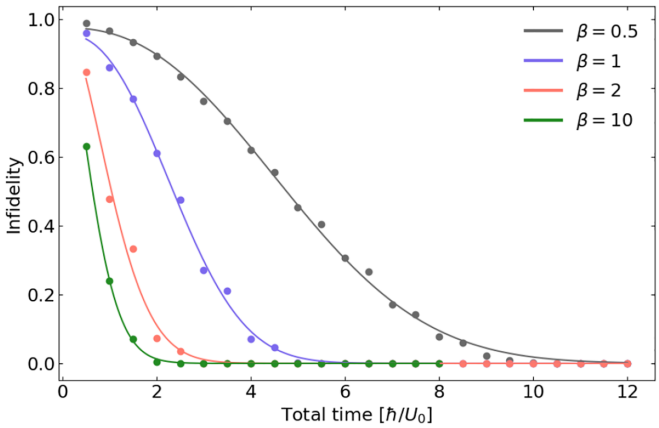

(a)

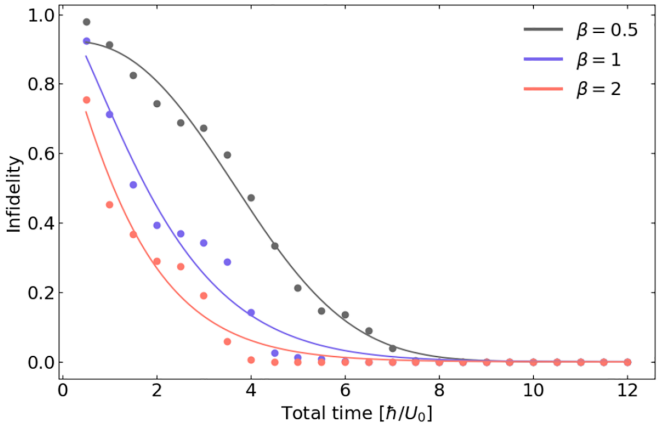

(b)

FIG. 5. Infidelity vs time curves for (a) $|0\rangle \rightarrow |2\rangle$ transfer with $\beta(x/a)^2$ modulation and (b) $|0\rangle \rightarrow |1\rangle$ transfer with $\beta(x/a)$ modulation. The strength of the β value are labeled in the plot legends. The individual data points are the best results of 2000 optimizations, and the line is a guide to the eye.

comparable to the case of the periodic perturbations but with transfer times reduced by up to a factor ∼5. Differently from the case of periodic perturbation, with quantum control it is possible to increase β, hence reducing significantly the transfer time, while keeping the population of higher levels negligible. All the transfer times reported on Table I correspond to experimental times of 5 s or less, which is feasible for state preparation prior to the experiments discussed in the following sections.

III. RESONANCE CASCADES

In this section we introduce the idea of using *resonance cascades* to study statements from number theory. That is, given a number-theoretical statement, we will first recast the statement or some of its corollaries as an assertion of an existence of an uninterrupted arithmetic progression. This arithmetic progression is a subsequence of a larger sequence of numbers (the principal sequence). The latter sequence will constitute the energy spectrum of a quantum system. The step

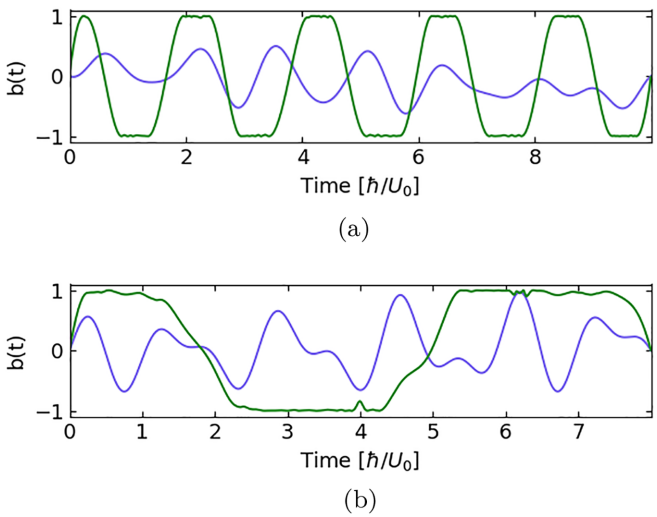

FIG. 6. Optimal controls $b(t)$ for (a) $\beta(x/a)^2$, $|0\rangle \to |2\rangle$ transfer and (b) $\beta(x/a)$, $|0\rangle \to |1\rangle$ transfer. Here $\beta = 0.5$. The blue (green) line denotes the initial (optimized) control.

between elements of the arithmetic subsequence in question will correspond to the frequency of a time-dependent perturbation. If the arithmetic progression is fully contained in the principal sequence, then the corresponding quantum system will be able to travel along the energy axis, exclusively via resonant transitions.

The following three examples are considered in this paper (also summarized in Table II):

(I) The number-theoretic statement: *The sequence of natural numbers* $\mathbb{N} = 1, 2, 3, \ldots$ *is closed under multiplication*.

Corollary to be studied: Given a natural number $\tilde{n}$, any power of it, $(\tilde{n})^m$, will be present in the sequence of natural numbers.

The principal sequence of numbers: $\ln(n)$ with $n = 1,\ 2,\ 3\ \ldots$.

The arithmetic progression: $m \ln(\tilde{n})$ with $m = 0,\ 1,\ 2,\ 3,\ \ldots$, with $\tilde{n}$ being a natural number.

The corresponding quantum system: One particle in a trap whose energy spectrum is proportional to the logarithms of natural numbers, $E_n^L = U_0 \ln(n),\ n = 1,\ 2, 3, \ldots$. The excitation frequency will be given by $\hbar\Omega = U_0 \ln \tilde{n}$.

(II) The number-theoretic statement: *The sequence of sums of two squares of integers is closed under multiplication* [Diophantus-Brahmagupta-Fibonacci identity [13] (Lemma 1, p. 142)].

Corollary to be studied: Given a sum of two squares $\tilde{s}$, any power of it, $(\tilde{s})^m$, will be present in the sequence of sums of two squares.

The principal sequence of numbers: $\ln(s_n)$ with $s_1 = 0^2 + 1^2 = 1,\ s_2 = 1^2 + 1^2 = 2,\ , s_3 = 0^2 + 2^2 = 4,\ s_4 = 1^2 + 2^2 = 5,\ s_5 = 2^2 + 2^2 = 8,\ \ldots$ [23].

The arithmetic progression: $m \ln(\tilde{s})$ with $m = 0,\ 1,\ 2,\ 3,\ \ldots$, and $\tilde{s}$ being a nonzero sum of two squares.

The corresponding quantum system: One particle in a trap whose energy spectrum is proportional to the logarithms of sums of two squares, $E_n^{L2} = U_0 \ln(s_n),\ n =$

TABLE II. Number-theoretic problems to be studied in this work, where $\mathbb{N} = 1, 2, 3, \ldots$ is the sequence of natural numbers and $\mathbb{N}_0 = 0, 1, 2, \ldots$ is the sequence of whole numbers (i.e., natural numbers including zero). In (II) we do not consider $0^2 + 0^2 = 0$ for technical reasons. Note the degeneracies in the principal sequence of numbers $w_{n,l}$ considered in (III). Preliminary numerical results for case (I) are published in Ref. [22].

Number-theoretic statement	Corollary to be studied	Principal sequence of numbers	Arithmetic progression	Corresponding quantum spectrum	Excitation frequency ($\hbar\Omega$)
(I) The sequence of natural numbers is closed under multiplication.	Given $\tilde{n} \in \mathbb{N}$, $\forall m \in \mathbb{N}_0$, $\tilde{n}^m \in \mathbb{N}$	$\ln(n)$, $n \in \mathbb{N}$.	$m \ln(\tilde{n})$, $\tilde{n} \in \mathbb{N}$, $m \in \mathbb{N}_0$	single-particle, $E_n^L = U_0 \ln(n)$, $n \in \mathbb{N}$	$U_0 \ln(\tilde{n})$
(II) The sequence S of sums of two squares of integers is closed under multiplication.	Given $\tilde{s} \in S$, $\forall m \in \mathbb{N}_0$, $\tilde{s}^m \in S$.	$\ln(s_n)$ with $s_n \in S$, $s_n \neq 0$	$m \ln(\tilde{s})$, $m \in \mathbb{N}_0$, and $\tilde{s} \in S$, $\tilde{s} \neq 0$	single particle, $E_n^{L2} = U_0 \ln(s_n)$, $s_n \in S$, $s_n \neq 0$	$U_0 \ln(\tilde{s})$
(III) Any even number greater than 2 is a sum of two primes.	Any even number greater than 4 is the sum of two primes greater than 2.	$w_{n,l}$ with $w_1 = 3 + 3 = 6$, $w_2 = 3 + 5 = 8$, $w_{3,1} = 5 + 5 = 10$, $w_{3,2} = 3 + 7 = 10$, $w_4 = 5 + 7 = 12,\ \ldots$	$2m$ with $m = 3,\ 4,\ 5,\ \ldots$	two interacting particles, each with $E_n = U_0 p_n$ where p_n are primes >2, i.e., 3, 5, 7, 11 …	$2U_0$

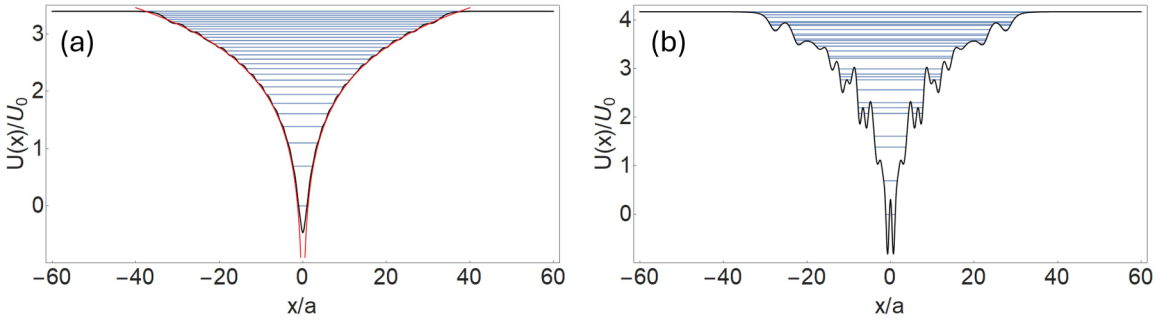

FIG. 7. Two potentials with a prescribed spectrum. (a) A potential whose lowest 30 energy levels are proportional to the logarithms of the first 30 natural numbers, as considered in Example (I). The red curve is its classical counterpart, Eq. (6). (b) A potential where the lowest 30 energy levels are proportional to the logarithms of the sums of two squares, considered in Example (II).

1, 2, 3, ... The excitation frequency will be given by $\hbar\Omega = U_0 \ln \tilde{s}$.

(III) The number-theoretic statement: *Any even number greater than 2 is a sum of two primes* [Goldbach conjecture [13] (p. 147)].

Corollary to be studied: Any even number greater than 4 is a sum of two primes greater than 2.

The principal sequence of numbers, with degeneracies: $w_{n,1}$ with $w_1 = 3+3 = 6$, $w_2 = 3+5 = 8$, $w_{3,1} = 5+5 = 10$, $w_{3,2} = 3+7 = 10$, $w_4 = 5+7 = 12$, ...

The arithmetic progression: $m \times 2$ with $m = 3, 4, 5, \ldots$.

The corresponding quantum system: Two interacting particles in a trap whose one-body energy spectrum, $E_n^P = U_0 p_n$, $n = 2, 3, 4, 5, \ldots$ is proportional to the prime numbers greater than 2, i.e., 3, 5, 7, 11 .... The excitation frequency will be given by $\hbar\Omega = 2U_0$.

Examples (I) and (II) require a trapping potential where the energy levels are logarithms of natural numbers and logarithms of the sequence of sums of two squares, respectively, as shown in Fig. 7. Example (III) requires two weakly interacting particles trapped in the prime number potential in Fig. 1. Example (I), which is to be regarded as a proof-of-principle, is studied in depth in Sec. IV. For examples (II) and (III), we outline ideas for future experiments in Sec. V.

IV. RESONANCE CASCADE PREDICATED ON THE CLOSENESS OF THE NATURAL SET UNDER MULTIPLICATION

A. The setup

Consider a one-body potential $U^L(x)$ whose lowest N_b bound state energies are given by

$$E_n^L = U_0 \ln n \qquad n = 1, 2, 3, \ldots, N_b. \tag{5}$$

Figure 7(a) shows this potential for $N_b = 30$. Similarly to the prime number potential of Sec. II, this potential is designed using supersymmetric methods [9]. As N_b increases, the potential converges to a smooth classical limit. This classical counterpart can be extracted using procedures developed in classical mechanics (see Sec. 12 in Ref. [24]). There exists a variety of classical potentials that can approximate our quantum potential; one of these is a logarithmic potential,

$$U_{\text{cl.}}^L(x) = U_0 \ln\left(\sqrt{\frac{2}{\pi}}\frac{x}{a}\right), \tag{6}$$

where $a \equiv \hbar/\sqrt{mU_0}$ (see Appendix A1).

Note that the existence of the classical limit of an artificially constructed potential with an *a priori* prescribed spectrum is not guaranteed. Figure 7(b) shows a potential whose first $N_b = 30$ energy levels are proportional to the first 30 integers that are equal to the sum of two squares. We see that as N_b increases, this potential retains its substantially quantum nature in that the small potential wells in Fig. 7(b) can be shown to contain only one or two eigenstates.

B. Protocol

Let us choose a natural number of interest, $\tilde{n}$, and its initial power, m_0. Our goal is to propose an effect that would be predicated on the presence of all powers of $\tilde{n}$ (up to a practical upper limit) in the set of natural numbers. To this end, consider a single atom (or an ensemble of noninteracting atoms) in an excited state $|n = \tilde{n}^{m_0}\rangle$, with $\tilde{n}^{m_0} < N_b$. Next, we apply a parametric perturbation

$$V(x, t) = \beta \cos(\Omega t)\, U^L(x), \tag{7}$$

where

$$\Omega = \frac{1}{\hbar} U_0 \ln(\tilde{n}), \tag{8}$$

with $\beta \ll 1$. The full Hamiltonian becomes

$$\hat{H}^L = \frac{\hat{p}^2}{2m} + (1 + \beta\cos(\Omega t)) U^L(x).$$

This perturbation will induce a resonance cascade, i.e., a cascade of resonant transitions between states,

$$|n=1\rangle \overset{\Omega}{\leftrightarrow} |n=\tilde{n}\rangle \overset{\Omega}{\leftrightarrow} |n=\tilde{n}^2\rangle \overset{\Omega}{\leftrightarrow} \ldots \overset{\Omega}{\leftrightarrow} |n=\tilde{n}^m\rangle \overset{\Omega}{\leftrightarrow} \ldots \overset{\Omega}{\leftrightarrow} |n=\tilde{n}^{m_0}\rangle \overset{\Omega}{\leftrightarrow} |n=\tilde{n}^{m_0+1}\rangle \overset{\Omega}{\leftrightarrow} \ldots, \tag{9}$$

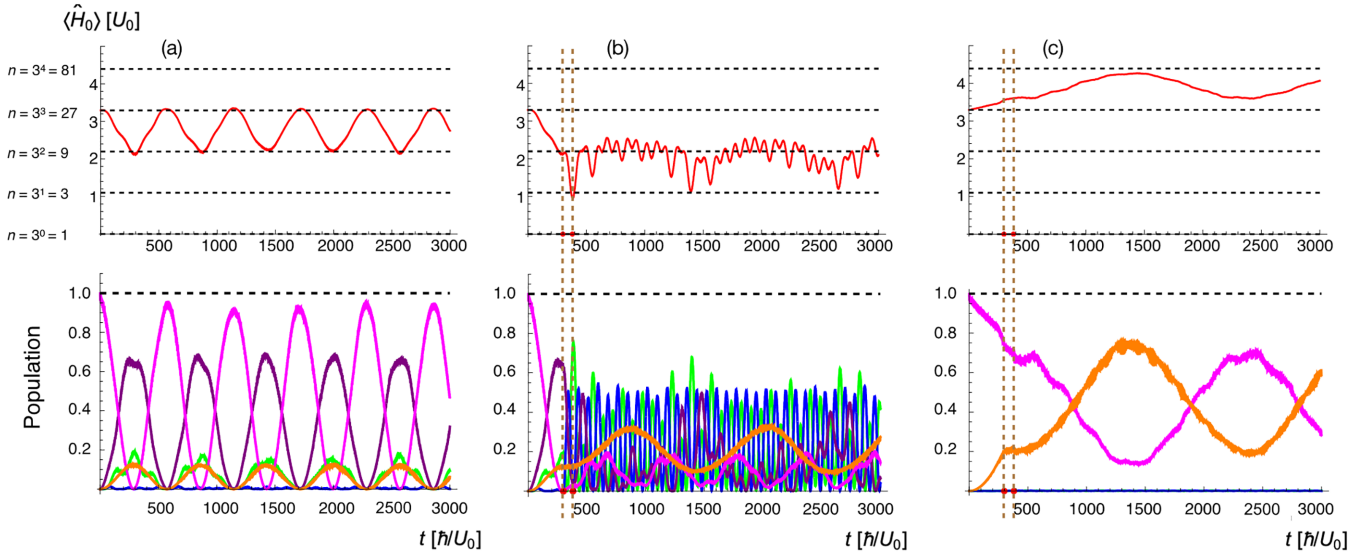

FIG. 8. A numerical experiment designed to verify if all powers of 3 are present in the set of natural numbers. A single atom is initially placed in the $|n = 27\rangle$ state of the potential $U^L(x)$ whose spectrum is given by $E_n^L = U_0 \ln(n)$ ($n = 1, 2, 3, \ldots, 120$). The atom is subjected to a periodic perturbation of the form $V(x, t) = \beta U^L(x) \cos(\Omega t)$, with $\beta = 0.3$, and $\Omega = \frac{1}{\hbar} U_0 \times \ln(\tilde{n})$, where $\tilde{n} = 3$. The upper panel shows the unperturbed energy of the system. The lower panel shows the population of the unperturbed eigenstates constituting the resonant cascade: $|n = 1\rangle$ (green), $|n = 3\rangle$ (blue), $|n = 9\rangle$ (purple), $|n = 27\rangle$ (magenta), and $|n = 81\rangle$ (orange); in all three cases and for all reported instances of time, these populations comprise no less than 80% of the total atomic population. (a) Mobility is impeded due to "dark-state" localization (Appendix B 1). Indeed, the lower panel shows that the time evolution is close to Rabi oscillations between $|n = 27\rangle$ and $|n = 9\rangle$. (b) In this numerical experiment, we introduce two "windows of silence" of a duration $\Delta t = \frac{\pi}{2\Omega}$, at $t = \{298.83, 380.31\} \times \hbar/U_0$ (red dots on the abscissa and dashed vertical lines), during which the perturbation is stopped and then restarted after a quarter of the perturbation period, at the phase it had just before the window. The windows are designed to break the "dark states" and in doing so, promote mobility along the energy axis. The level population indeed starts moving down in energy while remaining within the set of resonantly coupled energy levels $U_0 \times \log(n = 3^m)$. The lower panel shows that all five states comprising the resonance cascade become substantially populated. (c) A gedanken experiment where $n = 9$ is excluded from the set of natural numbers. At a technical level, we create a potential with a spectrum $E_n = U_0 \ln(n)$ ($n = 1, 2, 3, \ldots, 8, 11, 12, \ldots, 120$) where the $n = 9$ energy level is excluded. We also exclude the $n = 10$ level in order to preserve the relative parity of the remaining eigenstates. Such an exclusion can be seen to impede the mobility along the energy axis. In this experiment, we apply the same "windows of silence" as in (b). The lower panel shows that the time evolution is close to Rabi oscillations between $|n = 27\rangle$ and $|n = 81\rangle$.

which will cause the population to spread over energy levels in a resonant manner. An ability of our system to reach the $|n = 1\rangle$ state would serve as a "proof" that each of the numbers $1, \tilde{n}, \tilde{n}^2, \ldots, \tilde{n}^{m_0}$ belongs to the set of naturals.

Our first numerical experiment features the following set of parameters: the number of bound states N_b was set to 120, and we choose $\tilde{n} = 3$ and $m_0 = 3$ such that the initial state is $|n = 27\rangle$. The perturbation amplitude is $\epsilon = 0.3$. Figure 8(a) shows our results. While the members of the cascade, cf. Eq. (9), clearly dominated the population (see lower panel), the population was localized in the vicinity of $m = 3$ and $m = 2$.

In order to understand the origin of this localization, we analyze the behavior of the off-diagonal matrix elements of our perturbation, $|\langle n'|U^L|n\rangle|$, as shown in Fig. 9(a). We find an inverse-linear dependence on the magnitude of the quantum number difference, $|n' - n|$. This assertion is well supported by the large-$|n' - n|$ asymptotics of the semiclassical approximation for the matrix elements, as shown by Eq. (A12) in Appendix A4. We obtain

$$\langle n'|U^L|n\rangle \overset{|n'-n|\gg 1}{\approx} \begin{cases} (-1)^{\frac{n'-n}{2}-1} \frac{U_0}{|n'-n|} & \text{for} \quad n' - n \text{ even}, \\ 0 & \text{for} \quad n' - n \text{ odd}. \end{cases}$$

Numerically, we find a dependence

$$|\langle n'|U^L|n\rangle| \overset{|n'-n|\gg 1}{\approx} A \frac{U_0}{|n' - n|},$$

with $A = 0.80$ for $n = 60$, cf. Eq. (A13), while our analytic result (A12) predicts $A = 1$. This shows a good agreement between the semiclassical approximation and the numerical calculation for the matrix elements.

In terms of the cascade states, Eq. (9), an inverse linear dependence of the transition matrix elements on $|n' - n|$ leads to an exponential decay of the hopping constant within the cascade. We obtain

$$|\langle n' = \tilde{n}^{m+1}|U^L|n = \tilde{n}^m\rangle| \sim U_0 e^{-\gamma m},$$

with $\gamma = \ln(\tilde{n})$. Under a rotating-wave approximation, the system becomes a tight-binding model with the hopping coefficients J_m (between the mth and $m + 1$st sites, or states, in our model) that exponentially decay as a function of m:

$$\hat{H}_{\text{EL}} = -J_0 \sum_{m=-\infty}^{+\infty} e^{-\gamma m} \left(|m + 1\rangle\langle m| + |m\rangle\langle m + 1|\right). \quad (10)$$

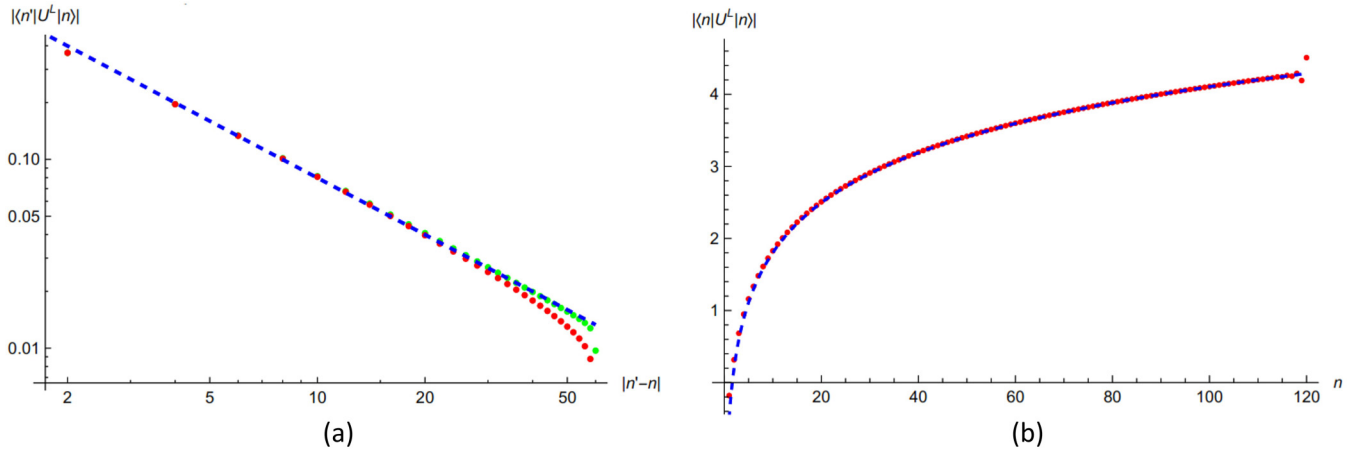

FIG. 9. Semiclassical approximation for the matrix elements of the perturbation (represented, in the case of a parametric excitation, by the potential energy) compared to the numerical results. (a) Absolute value of the off-diagonal matrix elements of the potential energy, $\langle n'|U^L|n = 60\rangle$, as a function of the absolute value of the index difference, $n' - n$. Only even values of $n' - n$ are represented, since the odd values vanish due to the parity selection rule. The green dots represent the numerical results for $n' > n$, while the red dots correspond to $n' < n$. The $\ln(n)$-spectrum potential used had $N_b = 120$ bound states. The blue dashed line is the semiclassical prediction $|\langle n'|U^L|n\rangle| \approx A\,U_0/|n' - n|$ [see Eq. (A13)] with the value of the fit parameter $A = 0.80$ representing the best fit for the data with $4 \leqslant |n' - n| \leqslant 30$. (b) Numerically computed diagonal matrix elements of the potential energy, $|\langle n|U^L|n\rangle|$ (red dots), in comparison with the virial formula (A14) (blue, dashed line); no fit parameters were used.

The coefficient J_0 in this exponential lattice model is then given by

$$J_0 = \frac{1}{2} U_0 \frac{A}{(\tilde{n} - 1)}.$$

In Appendix B we study the resulting lattice system in detail. Indeed, we find a localization for any eigenstate energy E. While a localization in the "classically forbidden" region of high m, where $|E| \gg J_m$ was expected, a localization in the direction of lower m, where $|E| \ll J_m$ requires an explanation. We find that in this region, the eigenstate wave function becomes a member of the kernel of the Hamiltonian, i.e., a state such that the action of the Hamiltonian on it is null (see Appendix B1). The structure of such a "dark state" (DS) wave function [25,26] is as follows (cf. Fig. 14). The population of the odd sites is zero, as the amplitudes of the even sites form a coherent superposition to ensure that there is no population of the odd sites when the Hamiltonian in Eq. (10) acts on such a superposition. On the other hand, since the even sites have unpopulated neighbors, the action of the Hamiltonian Eq. (10) on such a state is zero [27]. Finally, in Appendix B1, we show that the coherence of a dark state leads to an exponential decay of the population in space.

To promote mobility along the energy axis, we consider the following amendment to our protocol. Whenever localization occurs, we stop the excitation for a quarter of its period (i.e., for a time interval $\Delta t = \frac{\pi}{2\Omega}$) and then restart the excitation, maintaining the phase of the drive as it was in the beginning of this so-called *window of silence*. As a result, the free evolution during Δt flips the relative sign of the neighboring even sites, thus breaking the coherence of the dark-state tail. Figure 8(b) shows that this is indeed a valid strategy. With only two windows of silence we are able to transport the population towards the ground state while traveling exclusively through the resonance ladder. Thus this experiment demonstrates, via simulation, that all of the powers of 3 lower than or equal to $3^3 = 27$ are present in the set of natural numbers.

Finally, we simulate a fictitious universe where $3^2 = 9$ is not a natural number. In Fig. 8(c), we consider a potential with a spectrum similar to the simulation shown in Fig. 8(b) but with the $n = 9$ level excluded, along with the $n = 10$ level to preserve the relative parity of the remaining eigenstates. Using the same driving protocol as in Fig. 8(b), we note that the downward energy transfer stops at the missing levels, affirming the ability of our procedure to notice holes in energy-equidistant ladders of the quantum eigenstates [28].

In an experimental implementation, the dynamics shown in Fig. 8 will be observable in less than 10 s, i.e., on a similar timescale to the dynamics presented in Sec. II, even though the time axis in Fig. 8 extends to larger values compared to the time axis in the figures of Sec. II. The reason is as follows: The value of the energy scale U_0 is larger for the logarithmic potential than for the prime number potential. This is due to the cusplike shape of the logarithmic potential, which is narrower than the flatter profile of the prime number potential, leading to a larger spacing between the energy levels of the logarithmic potential. This larger energy scale thus gives a smaller time unit $\hbar/U_0$. Hence, the physical time span of Fig. 8 ends up being comparable to those of the protocols in Sec. II.

C. Discussion

For the simulations presented here, we used a parametric perturbation. We have previously considered power-law perturbations, such as the quadratic perturbation used in Sec. II, but we found that for power-law drives, the transition matrix elements change more rapidly over the cascade compared to the $|n' - n|^{-1}$ dependence for the case of the parametric perturbation. Hence power-law perturbations appear to be less favorable for cascades. However other choices of perturbation

could lead to a better behavior of the matrix elements, with the ideal perturbation being one that gives approximately constant matrix elements over the cascade. This will be an area of further investigation in future work.

Second, in the current scheme we position the windows of silence in an *ad hoc* manner. Finding the optimal number and timing of the windows required numerical experimentation. In the future, we would like to find a recipe that will be able to suggest the optimal sequence of the windows of silence without a need for numerical or empirical experiments.

V. FUTURE EXPERIMENTS WITH RESONANCE CASCADES

Building on the results of the previous section, here we propose that resonance cascades can be used to study other statements from number theory. In particular, we address the Diophantus-Brahmagupta-Fibonacci identity and the Goldbach conjecture, cases (II) and (III) of Table II.

A. Resonance cascade predicated on the validity of the Diophantus-Brahmagupta-Fibonacci identity

The set of natural numbers is not the only set of integers that is closed under multiplication. As follows from the Diophantus-Brahmagupta-Fibonacci identity [13] (Lemma 1, p. 142), the set of integers that are equal to the sums of two squares [see Eq. (11)] also has this property [29,30]. An example of a potential whose spectrum is proportional to the sequence in Eq. (11) is shown in Fig. 7(b).

Similarly to the case of a $\ln(n)$-spectrum potential shown in Fig. 7(a), the $\ln(s)$-spectrum potential,

$$\begin{aligned} E_n^{L2} &= U_0 \ln s_n \\ &\quad s_1,\ s_2,\ s_3,\ s_4,\ \ldots \\ &= (0^2+1^2),\ (1^2+1^2),\ (0^2+2^2),\ (1^2+2^2),\ \ldots \\ &\quad n = 1,\ 2,\ 3,\ \ldots,\ N_b. \end{aligned} \tag{11}$$

where the integers s are each the sum of two squares, will support unbounded cascades of resonant transitions for a single particle in the $\ln(s)$-spectrum potential. Such cascades require that the frequency of the perturbation must have the form

$$\Omega = \frac{1}{\hbar} U_0 \ln \tilde{s},$$

where $\tilde{s}$ is itself a sum of two squares. Note that for technical reasons, we exclude $0^2+0^2=0$ from the set in Eq. (11).

B. Resonance cascade predicated on the validity of the Goldbach conjecture

Unlike the $\ln(n)$-spectrum potential considered above, a one-body potential whose spectrum is given by the prime numbers has already been demonstrated theoretically and experimentally [9]. We examined state manipulation and control in this potential in Sec. II. As a slight modification, in this section, we will exclude 2 from the set of primes, given that 2 only enters in the Goldbach decomposition of 4 and not in the Goldbach decomposition of higher even numbers. Then, the potential will have the following one-body spectrum:

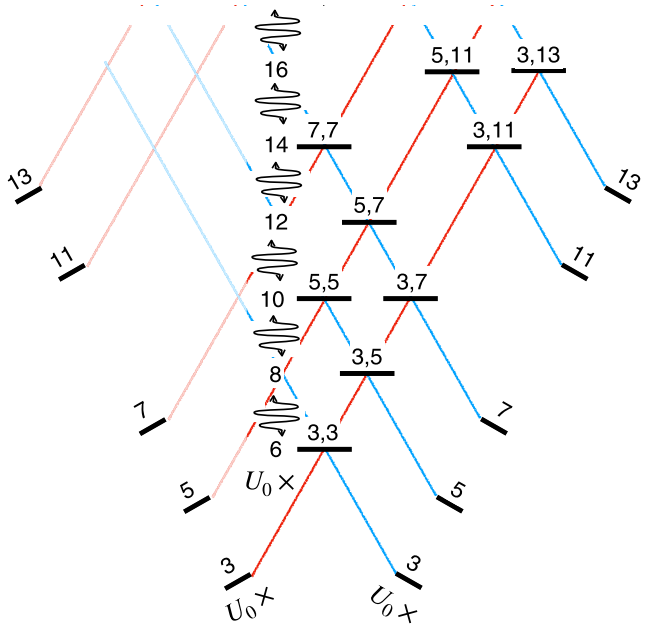

FIG. 10. Energy spectrum of two weakly interacting bosons in a p-spectrum potential. The energy levels, $E = U_0 \times 4,\ 6,\ 8,\ \ldots$, are formed by sums of two prime numbers, p_1 and $p_2 \geqslant p_1$. In the text, we suggest applying a weak periodic one-body resonant perturbation of frequency $2U_0/\hbar$. Up to the level $E = 38U_0$, the one-body transitions alone ensure the resonant upward mobility of the system, thanks to a proliferation of twin prime pairs. The gap between $E = 38U_0$ and $E' = 40U_0$, which is inaccessible by one-body processes, can be overcome by weakly mixing the original eigenstates using a two-body interaction. Finally, a complete upward mobility of the level population is predicated on the validity of Goldbach's conjecture.

$$\begin{aligned} E_n^{P} &= U_0 p_n \\ &\quad p_1,\ p_2,\ p_3,\ p_4,\ \ldots = 3,\ 5,\ 7,\ 11,\ \ldots \\ &\quad n = 1,\ 2,\ 3,\ \ldots,\ N_b. \end{aligned} \tag{12}$$

Consider two bosonic atoms in this p-spectrum trap (see Fig. 10). For the moment, let us set interactions to zero. Let us apply a weak *one-body* periodic perturbation $\hat{V}\cos(\Omega t)$ of frequency $\Omega = 2U_0/\hbar$. This perturbation changes the energy of one of the atoms by $2U_0$, while leaving the energy of the other atom unchanged. Let us start from the ground state, $|3,\ 3\rangle$, and explore the possibility of traveling infinitely high in energy via resonant transitions *only*.

Consider two energy-consecutive two-body eigenstates $|p_1,\ p_2\rangle$ and $|p_1',\ p_2'\rangle$, with

$$\begin{aligned} w &= p_1 + p_2, \\ w' &= p_1' + p_2', \\ p_2 &\geqslant p_1, \\ p_2' &\geqslant p_1', \\ &\text{and} \\ w' &= w + 2, \end{aligned}$$

where w is an even integer. The energies of these states are are given by $E = \hbar U_0 w$ and $E' = \hbar U_0 w' = E + 2U_0$, respectively. If at least one of the primes $p_1,\ p_2$ participating the Goldbach decomposition of w is a lower member of a twin prime pair (a "lower twin" from now on), where twin primes are a pair of primes separated by 2, then $|p_1,\ p_2\rangle$ and $|p_1',\ p_2'\rangle$ will be resonantly coupled with a nonzero matrix element. That is, the one-body nature of the perturbation imposes the following selection rule for the transition $w \to w' = w + 2$:

$$\begin{aligned} &p_1' = p_1 + 2 \text{ and } p_2' = p_2 \\ &\quad \text{or} \\ &p_2' = p_1 + 2 \text{ and } p_1' = p_2 \\ &\quad \text{or} \\ &p_1' = p_2 + 2 \text{ and } p_2' = p_1 \\ &\text{or} \\ &p_2' = p_2 + 2 \text{ and } p_1' = p_1. \end{aligned} \tag{13}$$

For the allowed transitions, the transition matrix element can be estimated as

$$\langle p_1',\ p_2'|\hat{V} \otimes \hat{I} + \hat{I} \otimes \hat{V}|p_1,\ p_2\rangle \sim \langle p'|\hat{V}|p\rangle,$$

where $\langle p'|\hat{V}|p\rangle$ is a typical one-body matrix element of $\hat{V}$.

The first one-body-forbidden transition occurs at

$$\begin{aligned} w &= 38 = 7 + 31 = 19 + 19 \\ w' &= 40 = 3 + 37 = 11 + 29 = 17 + 23, \end{aligned}$$

and it is not known yet whether the number of such transitions is infinite or finite. To break the selection rules in Eq. (13), one will need to add a second potential, e.g., a weak two-body interaction potential $\hat{V}^{(2)}$. In this case, the previously forbidden transition $|p_1,\ p_2\rangle \to |p_1',\ p_2'\rangle$ becomes weakly allowed. To first order in perturbation theory with respect to $\hat{V}^{(2)}$, the transition matrix element is estimated by

$$\begin{aligned} &\langle p_1',\ p_2'|\hat{V} \otimes \hat{I} + \hat{I} \otimes \hat{V}|p_1,\ p_2\rangle \\ &\quad \sim \frac{\langle p'|\hat{V}|p\rangle\langle p_I',\ p_{II}'|\hat{V}^{(2)}|p_I,\ p_{II}\rangle}{U_0}, \end{aligned} \tag{14}$$

where $\langle p_I',\ p_{II}'|\hat{V}^{(2)}|p_I,\ p_{II}\rangle$ is a typical two-body matrix element of $\hat{V}^{(2)}$.

In Appendix C, we prove that the number of two-body energy levels that require two-body interactions to be resonantly coupled with the next level above is infinite (equivalently, that there exists an infinite number of even numbers whose Goldbach decomposition does not involve lower twin primes). Finally, it may happen that for a given two-body energy level E, the required level above, with energy $E + 2U_0$, has no eigenstates. In the language of number theory, this would mean that the even number w' cannot be represented as a sum of two primes. However, that would contradict Goldbach's conjecture, which states that every even number greater than 2 is the sum of two prime numbers. Note that here, as noted previously, we consider an equivalent formulation where every even number greater than 4 is a sum of two primes, each greater than 2. If we assume that Goldbach's conjecture is valid, then we can expect that starting from the ground state of our system, we can reach any of its excited states via resonant transitions alone.

According to the preliminary study [22], the atomic population can be exclusively contained within a resonantly coupled subset of energy levels if the typical values of the off-diagonal matrix elements of the perturbation are of the order of $|\langle p'|\hat{V}|p\rangle| \sim 10^{-4} \times U_0$ or lower, with U_0 representing the typical level spacing. Such a stringent requirement reflects the fact that experimentally accessible perturbations contribute to both the desired transition matrix elements between the cascade states and the parasitic off-resonant shifts of the unperturbed energy levels. The resulting uppper bound on the value of $|\langle p'|\hat{V}|p\rangle|$ is a result of a compromise between the necessity to ensure the dominance of the resonant processes and the desire to minimize propagation time. Note that the corresponding parasitic level shift is a second-order perturbation theory effect, and as such, should be of the order of $|\langle p'|\hat{V}|p\rangle|^2/U_0 \sim 10^{-8} \times U_0$ or lower.

On the other hand, the two-body interaction, $\langle p_I',\ p_{II}'|\hat{V}^{(2)}|p_I,\ p_{II}\rangle$, is a time-independent perturbation, and it will affect the level shifts in the first order of the perturbation theory. Assuming that the resulting undesirable level shifts $|\langle p_I',\ p_{II}'|\hat{V}^{(2)}|p_I,\ p_{II}\rangle$ are also of the order of $10^{-8} \times U_0$, the resulting allowed values of the transition matrix element (14) become impractically small, of the order of $10^{-12} \times U_0$ or less. One way to overcome this difficulty will be to offset the two-body-interaction-induced level shifts using *a priori* corrections to the unperturbed energy levels. In this case, the matrix element (14) can, conceivably, reach a value comparable to one of the couplings between the regular two-body energy levels.

VI. CONCLUSIONS

In this paper we have examined two types of potentials, prime number potentials and logarithmic potentials, that are relevant for applications of quantum physics to number theory. First, we studied the case in which the system behaves as a two-level system due to the unequal spacing between the energy levels. We have shown that, starting from the ground state, we can prepare an individual excited state with high fidelity. Moreover, transfer time can be reduced with quantum control techniques, which allows for faster state preparation for the experiments we consider in the rest of this work.

Next, we outlined a strategy for studying problems of number theory using quantum systems. The strategy consists of reducing a number-theoretic statement to an assertion of the existence of an uninterrupted arithmetic subsequence in a sequence of numbers and subsequently finding a quantum system with an energy spectrum proportional to this sequence. The existence of an arithmetic subsequence is illustrated by a cascade of resonant transitions under a periodic perturbation.

In this spirit, we have studied the example of the closeness of the set of natural numbers under multiplication in great detail. In doing so, we identified a difficulty that may occur in several instances of our class of protocols: The hopping constants in the resulting resonance cascades exhibit a sharp dependence on the site number. As a result, the eigenstates become localized inhibiting mobility along the energy axis. Subsequently, we found a way to unlock the mobility, so far in

the downward direction only. The recipe calls for introducing a few specifically designed short windows of silence during which the perturbation is turned off. Hence this protocol requires, as the starting point, the preparation of an excited state of the potential. Such preparation could be performed using quantum optimal control methods like those presented in Sec. IIB. Due to the logarithmic scaling of the energy levels (which leads to continuum-like behavior at higher levels but relatively large energy spacings between, e.g., the ground and first excited state), we found that gradient-based methods like GRAPE [19] tend to fail. On the other hand, gradient-free methods like genetic algorithms or methods relying on the constrained optimization within a given basis, like the the CRAB [31] or GROUP [21] methods will likely succeed, and both methods have been shown to work for similar atomic state preparation problems, as for instance in Refs. [32–36].

In the future, we plan to work on further improving the quantum control schemes to transfer particles from low-energy to high-energy eigenstates. Effect of temperature, interactions and transverse degrees of freedom should be also studied in detail to optimize the efficiency of number-theory-inspired devices. We also plan to design schemes in which one starts from the ground state of the trap and ignites a resonance cascade propagating upward in energy. In this regard, preliminary results have been shown in related work [22]. We envisage that this will make a future experimental implementation easier. Experimentally, it is easier to prepare an atom in the ground state than in a well-defined excited state. Moreover, an upward-oriented resonance cascade may be readily detectable by counting atoms that leave the trap completely, as they reach the threshold between the bound and the continuous spectra. Hence atom loss would be a clear experimental signature of an uninterrupted cascade.

ACKNOWLEDGMENTS

H.K. and C.W. wish to acknowledge the computational facilities of the Advanced Computing Research Centre, University of Bristol [37]. H.K. was funded by the EPSRC CDT in Quantum Engineering (EP/SO23607/1). C.W. acknowledges funding from EPSRC under Grant No. EP/Y004728/1. M.O. was supported by the NSF Grant No. PHY-2309271. O.V.M. acknowledges the support by the DLR German Aerospace Center with funds provided by the Federal Ministry for Economic Affairs and Energy (BMWi) under Grants No. 50WM1957 and No. 50WM2250E. The authors thank the Institut Henri Poincaré (UAR 839 CNRS-Sorbonne Université) and the LabEx CARMIN (ANR-10-LABX-59-01) for their support. G.M. and A.T. thank the kind hospitality and support from the program "Out-of-equilibrium Dynamics and Quantum Information of Many-body Systems with Long-range Interactions" at KITP (Santa Barbara). G.M. acknowledges the grants PNRR MUR Project No. PE0000023-NQSTI and PRO3 Quantum Pathfinder.

A significant portion of this work was produced during the thematic trimester on "Quantum Many-Body Systems Out-of-Equilibrium" at the Institut Henri Poincaré (Paris): A.T., G.M., and M.O. are grateful to the organizers of the trimester, Rosario Fazio, Thierry Giamarchi, Anna Minguzzi, and Patrizia Vignolo, for the opportunity to be a part of the program.

DATA AVAILABILITY

The data that support the findings of this article are not publicly available. The data are available from the authors upon reasonable request.

APPENDIX A: THE ln(n)-SPECTRUM POTENTIAL: MATRIX ELEMENTS OF THE PERTURBATION

In this article, we are concerned with the design of an experimental protocol that can make apparent the existence of equidistant energy-level ladders. Our method of choice is the study of the mobility of an initially prepared quantum state along the energy axis under a resonant perturbation. The design process involves analyzing simple numerical and analytic models of the process; these appendixes are devoted to that goal.

In the main text, we suggest using a parametric drive for inducing a resonance cascade. In particular, given the potential $U^L(x)$ that produces a logarithmic spectrum, Eq. (5),

$$\begin{aligned} \hat{H} &= \frac{\hat{p}^2}{2m} + U^{\mathrm{L}}(x) \\ \hat{H}|n\rangle &= E_n|n\rangle \\ E_n &= U_0 \ln(n) \\ n &= 1,\ 2,\ 3,\ \ldots, \end{aligned}$$

we apply a perturbation

$$V(x,\ t) = \beta \cos(\Omega t) U^{\mathrm{L}}(x),$$

where

$$\Omega = U_0 \ln(\tilde{n}),$$

and $\tilde{n}$ is a natural number. Note also that in the main text, we supplement the $\cos(\Omega t)$ time dependence of the perturbation with a few quarter-period-long windows of silence, as a method to enhance the mobility along the energy axis.

In the view of the above, estimates for the matrix elements of the potential $\langle n'|U^L|n\rangle$ will become needed. These estimates are the goal of this appendix.

1. A logarithmic approximation to the ln(n)-spectrum potential

In classical mechanics, the solution to the problem of restoring a trapping potential from its frequency as a function of energy is well known [38]:

$$x(U) = \frac{1}{\sqrt{2m}} \int_{U(0)}^{U} \frac{dE}{\omega(E)\sqrt{U-E}},$$

where $\omega(E)$ is the oscillation frequency as a function of energy, $x(U)$ is the inverse of the potential function $U(x)$ for $x \geqslant 0$, $U(0)$ is the value of the potential at the origin, and the potential $U(x)$ is assumed to be an even function of x such that $U(-x) = U(x)$. On the other hand, given a quantum energy spectrum, E_n, the classical frequency can readily be extracted as

$$\omega = \frac{1}{\hbar} \frac{dE_n}{dn}. \tag{A1}$$

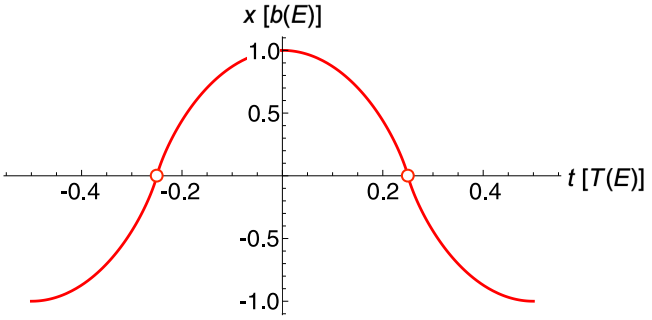

FIG. 11. Classical trajectory in a logarithmic potential. The time dependence of the x coordinate is given by a universal function, Eq. (A3), with the time t and x coordinate properly rescaled in terms of the period $T(E)$ and the amplitude $b(E)$. Note that the $x(t)$ curve experiences singularities at $t = \pm\frac{T}{4}$ where the particle velocity diverges logarithmically (open circles), but this is not readily visible in the plot. These singularities uniquely determine the high-frequency behavior of the Fourier components of the classical time dependence of the perturbation and, hence, its quantum matrix elements between the energy-distant unperturbed eigenstates.

In our case, the spectrum E_n is given by Eq. (5). Then the classical frequency as a function of energy becomes

$$\omega = \frac{1}{\hbar} U_0 e^{-\frac{E}{U_0}}. \tag{A2}$$

Now, assuming $U_0 = -\infty$, we get Eq. (6). Figure 7(a) shows a good agreement between the quantum $\ln(n)$-spectrum potential and its classical counterpart everywhere except for the substantially quantum region $|x| \lesssim a$ (whose size is comparable to the spatial extent of the quantum ground state).

2. Classical motion in a logarithmic potential

Classical equations of motion generated by the Hamiltonian

$$H^L_{\text{cl.}} = \frac{p^2}{2m} + U^L_{\text{cl.}}(x),$$

with $U^L_{\text{cl.}}(x)$ given by Eq. (6), can be readily solved, albeit implicitly:

$$t = \pm T(E) \begin{cases} +\frac{1}{4}\text{erf}\left(\sqrt{\ln\left(\frac{b(E)}{x}\right)}\right) & \text{for} \quad x > 0 \\ -\frac{1}{4}\text{erf}\left(\sqrt{\ln\left(\frac{-b(E)}{x}\right)}\right) + \frac{1}{2} & \text{for} \quad x < 0 \end{cases}, \tag{A3}$$

where $T(E) = (2\pi)/\omega(E)$ is the classical period, $\omega(E)$ is the classical frequency given by Eq. (A2), and

$$b(E) = \sqrt{\frac{\pi}{2}} a e^{\frac{E}{U_0}}$$

(see Fig. 11). At $t = \pm\frac{T}{4}$ particle's trajectory experiences logarithmic singularities

$$t \mp \frac{T}{4} \approx \mp \frac{T}{4\sqrt{\pi}} \frac{x}{b\sqrt{\ln\left(\frac{b}{|x|}\right)}}. \tag{A4}$$

In the vicinity of these singularities, the implicit relations in Eq. (A4) can be approximately inverted, using sequential iterations:

$$x_{n+1} = \mp 4\sqrt{\pi} b \left(\frac{t \mp \frac{T}{4}}{T}\right) \sqrt{\ln\left(\frac{b}{|x_n|}\right)},$$

$$x_0 = \mp 4\sqrt{\pi}\, b \left(\frac{t \mp \frac{T}{4}}{T}\right).$$

A comparison between the x_1 and x_2 iterations shows that

$$x(t) \approx x_1(t) = \mp 4\sqrt{\pi} b \left(\frac{t \mp \frac{T}{4}}{T}\right) \sqrt{\ln\left(\frac{T}{4\sqrt{\pi}\left(t \mp \frac{T}{4}\right)}\right)}, \tag{A5}$$

constitutes an accurate approximation to the true trajectory if

$$\sqrt{\ln\left(4\sqrt{\pi}\left(t \mp \frac{T}{4}\right)\right)} \ll \frac{T}{4\sqrt{\pi}\left(t \mp \frac{T}{4}\right)};$$

this condition is satisfied for

$$t \mp \frac{T}{4} \ll 0.1T.$$

In addition, let us observe the following. First, the asymptotic expansion of the erf function,

$$\text{erf}(y) \overset{y\gg 1}{=} 1 - e^{-y^2}\left\{-\frac{1}{\sqrt{\pi}y} + \frac{1}{2\sqrt{\pi}y^3} + \mathcal{O}\left(\frac{1}{y^5}\right)\right\},$$

shows that the approximation in Eq. (A4) is valid for

$$\ln\left(\frac{b}{|x|}\right) \gtrsim \frac{1}{2}.$$

On the other hand, the logarithmic singularity in the classical potential given by Eq. (6) is regularized in the quantum case [Fig. 7(a)], at $|x| \sim a$. This cutoff introduces the following bound:

$$\ln\left(\frac{b}{|x|}\right) \lesssim n,$$

where n is the typical eigenstate index of interest. In our case, $3 \lesssim n \lesssim 27$.

Observe that in Eq. (A4), another constant b, outside of the logarithm, depends on n exponentially. Accordingly, in these estimates, we will replace the logarithm appearing in Eq. (A4) by a constant L:

$$\ln\left(\frac{b}{|x|}\right) \to L$$
$$\frac{1}{2} \lesssim L \lesssim 27. \tag{A6}$$

Interestingly, in the estimates that follow, the actual value of the constant L turns out to be irrelevant. As it follows from our derivation below, the singularity in Eq. (A4) controls the behavior of the quantum off-diagonal matrix elements of the potential energy, for large differences between the quantum numbers.

3. Semiclassical approximation for the off-diagonal matrix elements of coordinate-dependent observables in one-dimensional traps: General results

In Ref. [39], one can find a set of results on a semiclassical approximation for off-diagonal matrix elements of quantum observables, both for the case of two close energies (Sec. 48 of Ref. [39]), and for two energies far apart (Sec. 51 in Ref. [39]). Before we address the question of the matrix elements of the potential $U^L(x)$ that generates the $\ln(n)$ spectrum given in Eq. (5), we will restate the main results in the former limit (shown to be relevant to our case), focusing on the case where the observable is a function of a coordinate.

Consider a one-dimensional quantum potential well with a potential energy $U(x)$. Let $\hat{A} = A(x)$ be the observable of interest. We will be interested in a semiclassical approximation to the matrix elements of the observable $\langle n'|\hat{A}|n\rangle$, where $|n\rangle$, $|n'\rangle$ indicate eigenstates of the system; the corresponding eigenenergies are $E_n, E_{n'}$.

In the classically allowed region, $E \geqslant U(x)$, the semiclassical approximation to the eigenstate wave function is

$$\psi_n(x) = \frac{2}{\sqrt{T(E_n)v(x,\,E_n)}} \cos\left(\frac{1}{\hbar}\int_{x_1(E_n)}^{x} p(x',\,E_n)dx' - \frac{\pi}{4}\right), \tag{A7}$$

where $T(E) = 2\pi/\omega(F)$ is the classical oscillation period as a function of energy, $\omega(E)$ is the classical frequency,

$$p(x,\,E) \equiv \sqrt{2m(E - U(x))}$$

is the magnitude of the classical momentum as a function of coordinate and energy, $v(x,\,E) \equiv p(x,\,E)/m$ is the the magnitude of the classical velocity, and $x_1(E)$ is the left turning point of particle's trajectory, i.e., the smallest of the two solutions of an algebraic equation $U(x) = E$. Within the accuracy of the semiclassical approximation, the wave function Eq. (A7) is normalized to unity. More specifically, its normalization integral is unity if one replaces the $\cos^2(\ldots)$ appearing there by $\frac{1}{2}$ (see Sec. 48 in Ref. [40]).

Next, we will introduce an energy E close to each of the energies E_n and $E_{n'}$, i.e., $E \approx E_n,\, E_{n'}$. A concrete choice for this energy is, to the leading order of the semiclassical approximation, irrelevant. The choice $E = (E_n + E_{n'})/2$ may, in some cases, improve accuracy beyond the leading order [41]; this choice also preserves the Hermitian nature of the matrix for the given observable. In this text, we will not commit to any particular convention.

For a matrix element of an observable $A(x)$, between an eigenstate $|n'\rangle$ and an eigenstate $|n\rangle$, we get:

$$\begin{aligned}
\langle n'|\hat{A}|n\rangle &= \int_{-\infty}^{+\infty} dx A(x)\psi_{n'}(x)\psi_n(x) \\
&\approx \frac{4}{T(E)}\int_{x_1(E)}^{x_2(E)} \frac{dx}{v(x,\,E)} A(x)\cos\left(\frac{1}{\hbar}\int_{x_1(E_{n'})}^{x} p(x',\,E_{n'})dx' - \frac{\pi}{4}\right)\cos\left(\frac{1}{\hbar}\int_{x_1(E_n)}^{x} p(x'',\,E_n)dx'' - \frac{\pi}{4}\right) \\
&\approx \frac{2}{T(E)}\int_{x_1(E)}^{x_2(E)} \frac{dx}{v(x,\,E)} A(x)\cos\left(\int_{x_1(E)}^{x} dx'(p(x,\,E_{n'}) - p(x,\,E_n))\right) \\
&\approx \frac{2}{T(E)}\int_{x_1(E)}^{x_2(E)} \frac{dx}{v(x,\,E)} A(x)\cos\left(\frac{1}{\hbar}\int_{x_1(E)}^{x} dx'(p(x',\,E_{n'}) - p(x',\,E_n))\right) \\
&\approx \frac{2}{T(E)}\int_{x_1(E)}^{x_2(E)} \frac{dx}{v(x,\,E)} A(x)\cos\left(\int_{x_1(E)}^{x} \frac{dx'}{v(x,\,E)}\omega(E)(n' - n)\right) \\
&= \frac{2}{T(E)}\int_{t_1}^{t_1+\frac{T(E)}{2}} dt\, A(x(t))\cos((t - t_1)\omega(E)(n' - n)) \\
&= \frac{1}{T(E)}\int_{t_1}^{t_1+\frac{T(E)}{2}} dt\, A(x(t))\cos((t - t_1)\omega(E)(n' - n)) + \frac{1}{T(E)}\int_{t_1}^{t_1+\frac{T(E)}{2}} dt\, A(x(t))\cos((t - t_1)\omega(E)(n' - n)) \\
&= \frac{1}{T(E)}\int_{t_1}^{t_1+\frac{T(E)}{2}} dt\, A(x(t))\cos((t - t_1)\omega(E)(n' - n)) + \frac{1}{T(E)}\int_{t_1-\frac{T(E)}{2}}^{t_1} dt\, A(x(t))\cos((t - t_1)\omega(E)(n' - n)).
\end{aligned} \tag{A8}$$

Above a semiclassical regime where the potential $U(x)$ does not change appreciably on the scale of the de Broglie wavelength, $\lambda_{\text{d-B}} \sim \hbar/p$, is assumed; we also used the relationship in Eq. (A1). Here and below, t_1 is the time when the particle reaches the left turning point, i.e., where $x(t_1) = x_1$. We also used $dt = dx/v(x,\,E)$. Finally, we used the fact the functions $A(x(t))$ and $\cos((n' - n)\omega(E)(t - t_1))$ are even with respect to a $(t - t_1) \to -(t - t_1)$ substitution and periodic with a

period $T(E)$. We arrive at the familiar semiclassical expression for the matrix elements of a coordinate-dependent observable $A(x)$ between two close energy levels [39],

$$\langle n'|\hat{A}|n\rangle \approx \frac{1}{T(E)}\int_{-\frac{T(E)}{2}}^{+\frac{T(E)}{2}} d\tau\, A(x(t_1+\tau))\cos(\Delta n\,\omega(E)\tau) \tag{A9}$$

$$\approx \frac{(-1)^{\Delta n}}{T(E)}\int_{-\frac{T(E)}{2}}^{+\frac{T(E)}{2}} d\tau'\, A(x(t_2+\tau'))\cos(\Delta n\,\omega(E)\tau'). \tag{A10}$$

Under this approximation, the matrix element in question becomes a cosine Fourier component of the time dependence of the classical counterpart. Here $\Delta n = n' - n$, $E \approx E_n$, $E_{n'}$, $t_1(t_2)$ are the left (right) turning point times and $\omega(E)$ is the frequency at energy E. Note that for this choice of the lower bound of the Fourier integral, the corresponding sine Fourier component vanishes.

4. Off-diagonal matrix elements of the potential energy for the ln(n)-spectrum potential

In this subsection we are going to use the semiclassical formula Eq. (A10) to estimate the off-diagonal matrix elements of the potential energy $\langle n'|U^L|n\rangle$ in conditions where the quantum number difference $n' - n$ is large compared to unity so that the existing intuition for asymptotic expansions of Fourier integrals is applicable [42] but small compared to n. The latter constraint ensures that the formula (A10) is still valid. Within the accuracy of the semiclassical approximation, we can replace the ln(n)-spectrum potential Eq. (5) with its classical counterpart Eq. (6). The classical trajectory is given by Eq. (A3).

According to Ref. [42], at large orders of a Fourier expansion, the Fourier components are dominated by the singularities in the time dependence. In our case, we are dealing with logarithmic singularities. Indeed, substituting the approximation Eq. (A5) to the potential Eq. (6) and using the substitution Eq. (A6), one gets

$$U^L_{\text{cl.}}(x(t)) \overset{t\approx\mp\frac{T}{4}}{\approx} U_0 \ln\left(4\sqrt{2}\left(\frac{b}{a}\right)\sqrt{L}\left(\frac{\left|t\mp\frac{T}{4}\right|}{T}\right)\right). \tag{A11}$$

To estimate the Fourier integral in Eq. (A10) at large quantum number differences ($1 \ll |n' - n| \ll n$), we extend the integral to the full axis of time, use the approximation in Eq. (A11), and introduce an ultraviolet cutoff, shown later to be removable. The following integral emerges:

$$\lim_{\lambda\to 0}\int_{-\infty}^{+\infty} d\tau\, \exp(i\tilde{\Omega}\tau)\exp(-\lambda|\tau|)\ln(\sigma|\tau|) = -\frac{\pi}{|\tilde{\Omega}|}.$$

The off-diagonal matrix elements of the potential can be estimated as

$$\langle n'|U^L|n\rangle \overset{|n'-n|\gg 1}{\approx} \begin{cases} (-1)^{\frac{n'-n}{2}-1}\frac{U_0}{n'-n} & \text{for} \quad n'-n = \text{even} \\ 0 & \text{for} \quad n'-n = \text{odd}. \end{cases} \tag{A12}$$

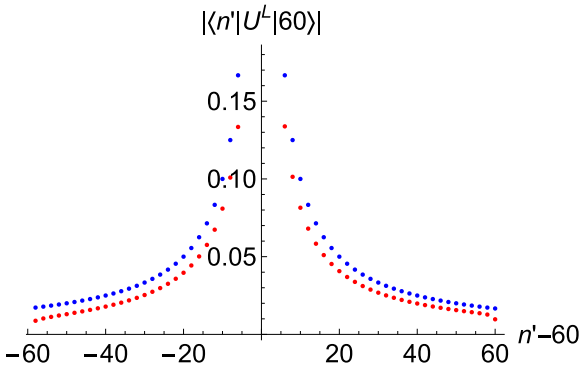

FIG. 12. A more complete presentation of the off-diagonal matrix elements of the perturbation (again represented, in the case of a parametric excitation, by the potential energy). This figure is supplementary to the one presented in Fig. 9(a). Here the full information about the sign the quantum number differences $n' - n$ is given. Only even values of $n' - n$ are represented, since the odd values vanish due to parity. The red dots represent numerical results. The ln(n)-spectrum potential used had $N_b = 120$ bound states. We also present the theoretical prediction (A12) that contains no fit parameters (blue dots).

A comparison with the numerical results shown in Fig. 12 shows that while Eq. (A12) captures the overall scaling,

$$|\langle n'|U^L|n\rangle| \overset{|n'-n|\gg 1}{\approx} A\,\frac{U_0}{|n'-n|}, \tag{A13}$$

it overestimates the coefficient A by 25%, predicting that $A = 1$ instead of the numerically obtained $A = 0.80$ [cf. Fig. 9(a)].

5. Diagonal matrix elements of the potential energy

For completeness, we present the semiclassical approximation for the diagonal matrix elements of the potential energy. Again, within the accuracy of the semiclassical approximation, we can replace the ln(n)-spectrum potential Eq. (5) with its classical counterpart Eq. (6).

Generally, diagonal matrix elements of observables are approximated using classical temporal averages. In our case, however, a virial theorem that has been previously applied to a logarithmic potential in Ref. [43] allows us to avoid the temporal average integrals. Using the result obtained in Ref. [43], we get:

$$\langle n|U^L|n\rangle \approx U_0 \ln(e^{-\frac{1}{2}}n). \tag{A14}$$

Figure 9(b) shows an excellent agreement between our prediction and *ab initio* results for a ln(n)-spectrum potential with $N_b = 120$ bound states.

APPENDIX B: THE EXPONENTIAL LATTICE

The goal of this appendix is to develop a theory for a quantum infinite one-dimensional lattice whose hopping coefficients decay exponentially in space. This model is relevant to the problem of a parametric excitation of the ln(n)-spectrum potential. In particular, using the exponential lattice model, we were able to identify the source of a localization in the space of the unperturbed eigenstates and devise the ways to break such a localization.

Consider the following one-body Hamiltonian:

$$\hat{H}_{\rm EL} = -J_0 \sum_{m=-\infty}^{+\infty} e^{-\gamma m} \left(|m+1\rangle\langle m| + |m\rangle\langle m+1|\right), \quad \text{(B1)}$$

where m are the indices of the lattice sites and γ is a positive constant. Below, we will discuss the solutions to the time-independent Schrödinger equation,

$$-J_0 e^{-\gamma m}(e^{\gamma}\psi_{m-1} + \psi_{m+1}) = E\psi_m$$
$$m = 0, \pm 1, \pm 2, \ldots, \quad \text{(B2)}$$

where ψ_m is the coordinate representation of an eigenstate

$$|\psi\rangle = \sum_{m=-\infty}^{+\infty} \psi_m |m\rangle$$

with an energy E,

$$\hat{H}_{\rm EL}|\psi\rangle = E|\psi\rangle.$$

For reasons that will become clear below, we have to start our discussion not from the eigenenergies but from the $m \to -\infty$ behavior of the eigenstates. We will proceed to the analysis of the spectrum, followed by by the $m \to +\infty$ asymptotic behavior.

1. Eigenfunctions in the "dark-state" region, $m \to -\infty$

Consider an eigenstate $|\psi\rangle$ with an energy E. At

$$m \ll \frac{1}{\gamma} \ln\left(\frac{J_0}{|E|}\right),$$

where $|E| \ll J_m$, the coefficients in front of the wave-function components $\psi_{m\pm1}$ in the Schrödinger equation Eq. (B2) exponentially explode, reducing the problem to finding the kernel, i.e., the dark state DS [25,26], of the Hamiltonian in Eq. (B1), i.e., where

$$\hat{H}_{\rm EL}|\psi_{\rm DS}\rangle = 0, \quad \text{(B3)}$$

or

$$e^{\gamma}(\psi_{\rm DS})_{m-1} + (\psi_{\rm DS})_{m+1} = 0,$$
$$m = m_{\rm DS}, m_{\rm DS}-1, m_{\rm DS}-2, \ldots. \quad \text{(B4)}$$

Here and below, $m_{\rm DS}$ is the right boundary of the zone of validity of the "dark-state" approximation in Eq. (B4), and $J_m \equiv J_0 e^{-\gamma m}$.

The wave function $(\psi_{\rm DS})_m$ can be immediately found to be

$$\psi_m \overset{m\to-\infty}{\approx} (\psi_{\rm DS})_m$$
$$(\psi_{\rm DS})_m = \begin{cases} (-1)^{\frac{m_{\rm DS}-m}{2}} e^{-\gamma\frac{m_{\rm DS}-m}{2}}\psi_{m_{\rm DS}} & \text{for} \quad m-m_{\rm DS} = \text{even} \\ 0 & \text{for} \quad m-m_{\rm DS} = \text{odd} \end{cases}$$
$$m = m_{\rm DS}, m_{\rm DS}-1, m_{\rm DS}-2, \ldots, \quad \text{(B5)}$$

where $\psi_{m_{\rm DS}}$ is the value of the *exact* eigenfunction at $m_{\rm DS}$ and is presumed to be known. Expectedly, in terms of lattices with constant hopping coefficients, this state can be interpreted a superposition of the two zero-energy plane waves with momenta $\pm\pi/2$.

Note the following, however. As m tends to $-\infty$, the wave function in Eq. (B5) decays as $e^{\gamma\frac{m}{2}}$, while the matrix elements of the Hamiltonian in Eq. (B1) explode more quickly, i.e., as $e^{-\gamma m}$. The only reason why the energy of the eigenstate does not diverge is the destructive interference between the two terms in Eq. (B4).

Imagine now that one decides to truncate the lattice at some negative position $m_{\rm left}$, in such a way that the allowed values of the coordinate m now span the range $m = m_{\rm DS}, m_{\rm DS}-1, m_{\rm DS}-2, \ldots, m_{\rm l}+1, m_{\rm left}$. The norm of the wave function in Eq. (B5) converges to a finite value for $m_{\rm left} \to -\infty$. Hence in this limit, the wave function remains finite. However, in the same limit, the left-hand side of Eq. (B3) will exponentially explode,

$$\hat{H}_{\rm EL}|\psi_{\rm DS}\rangle = -J_0 e^{-\gamma m_{\rm left}}(-1)^{\frac{m_{\rm DS}-(m_{\rm left}+1)}{2}} e^{-\gamma\frac{m_{\rm DS}-(m_{\rm left}+1)}{2}}\psi_{m_{\rm DS}}$$
$$\propto e^{+\gamma\frac{|m_{\rm left}|}{2}},$$

unless $m_{\rm left}$ and $m_{\rm DS}$ have the same parity, implying that $m_{\rm DS} - m_{\rm left}$ is even.

We arrive at the following conclusion: In the problem at hand, extending our lattice to $m = -\infty$ may produce unphysical eigenstates. Hence, we suggest the following amendment to our model: We will continue being interested in the eigenstates that are localized far away from the left boundary $m_{\rm left}$, rendering the actual position of this boundary irrelevant. However, the *parity* of $m_{\rm left}$ will remain important. Without loss of generality, we may assume that $m_{\rm left}$ is even. Finally, using the fact that $m_{\rm DS} - m_{\rm left}$ must be even, we establish the following rule: The infinite lattice solutions of the Schrödinger equation in Eq. (B2) must be *postselected* in such a way that only the eigenstates with the "dark-state" asymptotic behavior Eq. (B5) where $m_{\rm DS}$ is even are kept. This rule plays an important role in the next subsection.

2. The $+E \leftrightarrow -E$ symmetry, translational invariance, and the energy spectrum

Consider the Schrödinger equation in Eq. (B2). Two properties of the spectrum can be proven.

Property B1 (Positive-negative energy parity). Let $\psi_m^{(+)}$ be a solution of the eigenvalue problem Eq. (B2) corresponding to an eigenenergy $E = E^{(+)}$. Then the eigenstate-eigenenergy pair

$$\psi_m^{(-)} = (-1)^m \psi_m^{(+)}$$
$$E = E^{(-)} = -E^{(+)} \quad \text{(B6)}$$

is also a solution of Eq. (B2). The statement will remain valid if the infinite lattice is reduced to a ray or a line segment bounded by a Dirichlet boundary condition.

Proof. Indeed, substituting $\psi_m^{(-)}$ to Eq. (B2), we get

$$-J_0 e^{-\gamma m}\left(e^{\gamma}\psi_{m-1}^{(-)} + \psi_{m+1}^{(-)}\right)$$
$$\overset{(B6)}{=} -J_0 e^{-\gamma m}\left(e^{\gamma}(-1)^{m-1}\psi_{m-1}^{(+)} + (-1)^{m+1}\psi_{m+1}^{(+)}\right)$$
$$= -J_0 e^{-\gamma m}(-1)(-1)^m\left(e^{\gamma}\psi_{m-1}^{(+)} + \psi_{m+1}^{(+)}\right)$$
$$\overset{(B2)}{=} (-1)(-1)^m E^{(+)}\psi_m^{(+)}$$
$$\overset{(B6)}{=} E^{(-)}\psi_m^{(-)}.$$

■

Property B2 (Translational invariance). Let $\psi_m^{(\Delta m=0)}$ be a solution of the eigenvalue problem Eq. (B2) corresponding to an eigenenergy $E = E^{(\Delta m=0)}$. Then the eigenstate-eigenenergy pair

$$\begin{aligned}\psi_m^{(\Delta m)} &= \psi_{m-\Delta m}^{(\Delta m=0)} \\ E = E^{(\Delta m)} &= e^{-\gamma \Delta m} E^{(\Delta m=0)}\end{aligned} \tag{B7}$$

is also a solution of Eq. (B2).

Proof. Again, substituting $\psi_m^{(\Delta m)}$ to Eq. (B2), we get

$$\begin{aligned}&-J_0 e^{-\gamma m}\left(e^{\gamma}\psi_{m-1}^{(\Delta m)} + \psi_{m+1}^{(\Delta m)}\right) \\ &\overset{(B7)}{=} -J_0 e^{-\gamma m}\left(e^{\gamma}\psi_{m-\Delta m-1}^{(\Delta m=0)} + \psi_{m-\Delta m+1}^{(\Delta m=0)}\right) \\ &= -J_0 e^{-\gamma\,\Delta m} e^{-\gamma(m-\Delta m)}\left(e^{\gamma}\psi_{m-\Delta m-1}^{(\Delta m=0)} + \psi_{m-\Delta m+1}^{(\Delta m=0)}\right) \\ &\overset{(B2)}{=} e^{-\gamma\,\Delta m} E^{(\Delta m=0)}\psi_{m-\Delta m}^{(\Delta m=0)} \\ &\overset{(B7)}{=} E^{\Delta m}\psi_m^{(\Delta m)}.\end{aligned}$$

■

The Property B2 may seem paradoxical at first, as at may seem to imply, in combination with the Property B1 that there are twice as many eigenstates of the Hamiltonian as there are lattice sites. This apparent paradox is resolved in Sec. B 1. As we show there, a model given by Eq. (B1) on an infinite lattice is not physical, as it is not a limit of a problem on a ray of sites to the right of a Dirichlet boundary. However, an infinite lattice model where the eigenstates are postselected in such a way that only the states that in the limit $m \to -\infty$ develop nodes at the *odd* sites are kept represents a faithful

$$\begin{aligned}m_{\text{left}} &\to -\infty \\ m_{\text{left}} &= \text{even}\end{aligned}$$

limit of a ray with a Dirichlet boundary at m_{left}. More precisely, we assume that $\psi_{m_{\text{left}}-1} = 0$ at the $(m_{\text{left}} - 1)$th site. This consideration leads to the following amendment to the Property B2:

$$\Delta m = \text{even}. \tag{B8}$$

3. Eigenfunctions in the "classically forbidden" region, $m \to +\infty$

In this subsection, we will be interested in the region of space where

$$|E| \gg J_m, \tag{B9}$$

or

$$m \gg \frac{1}{\gamma}\ln\left(\frac{J_0}{|E|}\right).$$

If one forgets about the spatial dependence of J_m for a moment, then this area of space corresponds to a "classically forbidden" (CF) region where no waves can propagate. One would expect the wave function to develop an exponentially decaying tail instead. Furthermore, we will assume that the spatial variation of the hopping coefficient is slow in comparison with the spatial variation of the eigenstates. This is a domain of the parameter space where a semiclassical approximation can be used [39]. We will verify the validity of this assumption *a posteriori*.

Consider first the case where $E > 0$. If the hopping coefficient were a constant, $\bar{J}$, then the exponentially decaying solution of the Schrödinger equation Eq. (B2) would have the form

$$(\psi_{J_m=\bar{J}})_m = (-1)^{m-m_{\text{CF}}} e^{-\bar{\kappa} m}\psi_{m_{\text{CF}}}, \tag{B10}$$

where m_{CF} is the (left) boundary of the area of validity of the CF region approximation, $\psi_{m_{\text{CF}}}$ is the value of the *exact* eigenfunction at m_{CF}, and

$$\bar{\kappa} = \operatorname{arccosh}\left(\frac{E}{2\bar{J}}\right) \overset{|E|\gg\bar{J}}{\approx} \ln\left(\frac{E}{\bar{J}}\right).$$

To first order of the semiclassical approximation [39], the $\bar{\kappa} m$ under the exponent in (B10) is modified as

$$\bar{\kappa} m \to \sum_{m'=m_{\text{CF}}}^{m-1} \kappa_{m'},$$

with $\kappa_m \equiv \ln\left(\frac{E}{J_m}\right)$. After straightforward manipulation (see Appendix B4 for details), we get the following $m \to +\infty$ approximation, still restricted to positive energies, $E > 0$:

$$\begin{aligned}\psi_m &\overset{m\to+\infty}{\approx} (\psi_{\text{CF}})_m \\ (\psi_{\text{CF}})_m &= (-1)^{m-m_{\text{CF}}}\left(\frac{\sqrt{J_{m_{\text{CF}}}J_{m-1}}}{E}\right)^{m-m_{\text{CF}}}\psi_{m_{\text{CF}}} \\ m &= m_{\text{CF}},\ m_{\text{CF}}+1,\ m_{\text{CF}}+2,\ \ldots.\end{aligned}$$

The case of negative energies, $E < 0$, can be evaluated in a similar fashion. The only difference between the two signs of energies is that at the negative energies, there is no sign-alternating factor in the expression analogous to Eq. (B10).

Finally, an expression that covers both signs of energy reads

$$\begin{aligned}\psi_m &\overset{m\to+\infty}{\approx} (\psi_{\text{CF}})_m \\ (\psi_{\text{CF}})_m &= \begin{Bmatrix}(-1)^{m-m_{\text{CF}}} & \text{for} & E>0\\ 1 & \text{for} & E<0\end{Bmatrix} \\ &\quad\times\left(\frac{\sqrt{J_{m_{\text{CF}}}J_{m-1}}}{|E|}\right)^{m-m_{\text{CF}}}\psi_{m_{\text{CF}}} \\ m &= m_{\text{CF}},\ m_{\text{CF}}+1,\ m_{\text{CF}}+2,\ \ldots.\end{aligned} \tag{B11}$$

Let us finally assess the validity of the semiclassical approximation. According to Ref. [39], the semiclassical approximation is valid when the de-Broglie wavelength, $\lambda_{\text{d-B}}$, does not change appreciably over a length comparable to itself:

$$\frac{d\lambda_{\text{d-B}}}{dm} \ll 1.$$

In our case,

$$\lambda_{\text{d-B}} \sim \frac{1}{\kappa_m} \sim \frac{1}{\gamma(m-\tilde{m})},$$

with $\tilde{m} = -\frac{1}{\gamma}\ln(\frac{|E|}{J_0})$ is the location where the hopping coefficient is comparable to the magnitude of energy. The condition of validity of the approximation becomes

$$|E| \gg e^{\sqrt{\gamma}} J_m. \tag{B12}$$

Notice that this condition is more restrictive than the condition in Eq. (B9) for the CF region.

4. Derivation of Eq. (B11) for the eigenstate wave functions in the CF region

In this subsection we will derive the WKB approximation for the exponential lattice which leads to Eq. (B11). We will follow Bremmer's method as described in Ref. [44]. Since in the CF region, the spatial dependence of the hopping coefficient is slow, we divide the domain of interest into regions, not necessarily of the same size, with an approximately constant J_n in each region. The right boundary of each region is labeled by n_j, and the difference in magnitudes between the J_j in neighboring regions is small.

We consider the scattering problem with a step at n_j. The hopping coefficient to the left is J_L and to the right is J_R. To the right of the step the wave function is a decaying exponential with wave number κ_R, and to the left κ_L. The transmission coefficient is found to be

$$t_{n_j} = \frac{J_L(e^{\kappa_L} - e^{-\kappa_L})}{J_L e^{\kappa_L} - J_R e^{-\kappa_R}} e^{(\kappa_R - \kappa_L)n_j}.$$

To evaluate the wave function at some later point, we neglect reflection coefficients, which are very small in magnitude. We are free to choose the size of the regions in our domain, and more importantly their end points, so we may choose the end point of the final region, n_N, to be at the lattice point where we wish to evaluate the wave function. There the wave function is approximated by

$$\psi_{n_N} = e^{-\kappa_{n_{N+1}} n_N} \prod_{j=0}^{N-1} \frac{J_{n_j}(e^{\kappa_{n_j}} - e^{-\kappa_{n_j}})}{J_{n_j} e^{\kappa_{n_j}} - J_{n_{j+1}} e^{-\kappa_{n_{j+1}}}} e^{(\kappa_{n_{j+1}} - \kappa_{n_j})n_j}.$$

Since the difference between neighboring J_n is small,

$$\frac{J_{n_j}}{J_{n_{j+1}}} = 1 + \epsilon_j, \quad |\epsilon_j| \ll 1.$$

Then, to first order in ϵ_j,

$$\frac{J_{n_j}(e^{\kappa_{n_j}} - e^{-\kappa_{n_j}})}{J_{n_j} e^{\kappa_{n_j}} - J_{n_{j+1}} e^{-\kappa_{n_{j+1}}}} = \sqrt{\frac{J_{n_j} \sinh \kappa_{n_j}}{J_{n_{j+1}} \sinh \kappa_{n_{j+1}}}},$$

which becomes a telescoping series when the product is taken, leaving

$$\psi_{n_N} = \sqrt{\frac{J_{n_0} \sinh \kappa_{n_0}}{J_{n_{N-1}} \sinh \kappa_{n_{N-1}}}} e^{-\kappa_{n_{N+1}} n_N} \prod_{j=0}^{N-1} e^{(\kappa_{n_{j+1}} - \kappa_{n_j})n_j}.$$

The remaining exponential terms can be rewritten in terms of a sum, so that

$$\psi_{n_N} = \sqrt{\frac{J_{n_0} \sinh \kappa_{n_0}}{J_{n_{N-1}} \sinh \kappa_{n_{N-1}}}} e^{-n_0\kappa_0 + \sum_{j=1}^{N-1}(n_{j-1} - n_j)\kappa_j}.$$

We can now restore the κ_j associated with particular lattice points, so the WKB approximation for the wave function at a particular lattice point m becomes

$$\psi_m = \sqrt{\frac{J_{m_0} \sinh \kappa_{m_0}}{J_{m-1} \sinh \kappa_{m-1}}} e^{-m_0\kappa_0 - \sum_{j=1}^{m-1} \kappa_j}.$$

Next we invoke Eq. (B9), the condition that $|E| \gg J_m$. We consider propagation only within the classically forbidden region, so $m_0 = m_{\rm cf}$, and the summation in the exponent is now

$$\sum_{j=m_{CF}}^{m-1} \kappa_j.$$

To first order in J_m/E, this reduces the expression for the wave function to

$$(\psi_{\rm CF})_m = e^{-m_{\rm CF}\kappa_{\rm CF}} \left(\frac{J_0}{|E|} e^{-\gamma(m_{\rm CF} + m - 1)/2} \right)^{m - m_{\rm CF}},$$

which can be rewritten using the definition of J_m to read

$$(\psi_{\rm CF})_m = \left(\frac{\sqrt{J_{m_{\rm CF}} J_{m-1}}}{|E|} \right)^{m - m_{\rm CF}} \psi_{m_{\rm CF}}. \tag{B13}$$

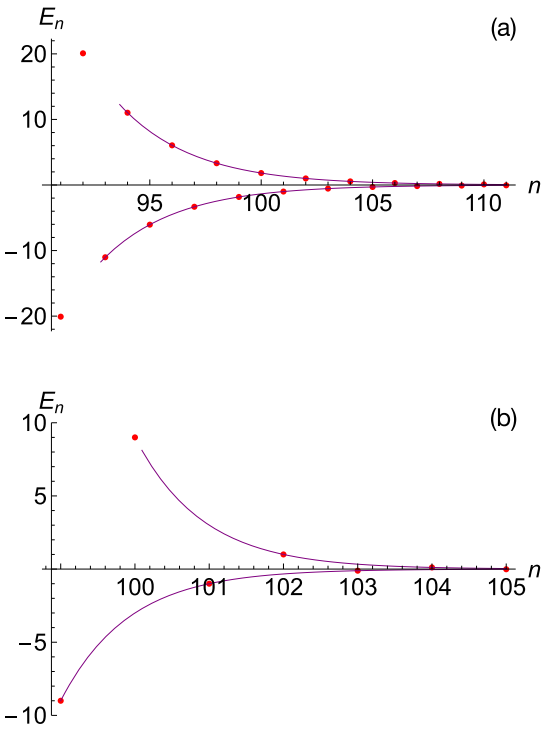

FIG. 13. Exponential lattice: Energy spectra. The coupling constant decay rate is given by (a) $\gamma = 0.3$ and (b) $\gamma = \ln(3)$, respectively. Spectra are ordered in the descending order of the magnitude of energy, and energy is measured in the units of J_0. The red dots show the numerical prediction, and the solid thin lines represent the predictions in Eqs. (B7) and (B8). Notice also that for any magnitude of eigenenergy, both signs of the eigenenergy are present in the spectrum, in agreement with Eq. (B6). Finally, the presence of the $E = \pm J_0$ levels for both values of γ remains unexplained.

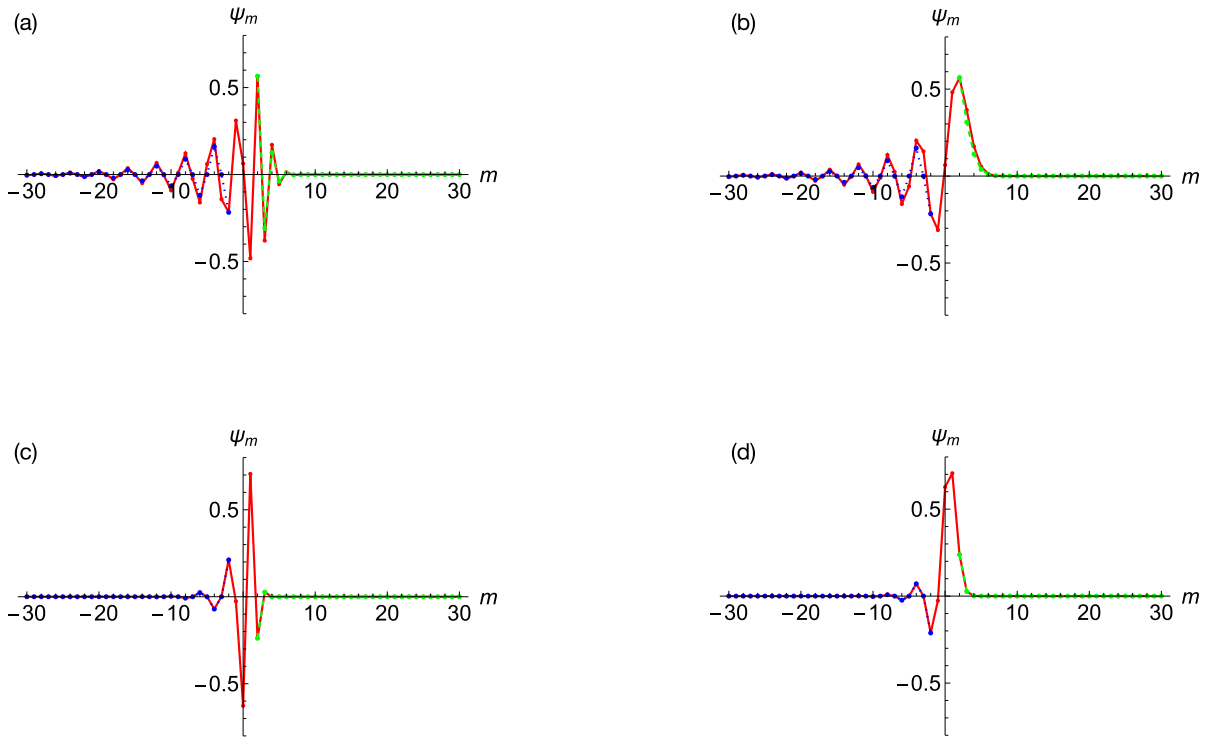

FIG. 14. Exponential lattice eigenstates. The $E = +J_0$ [(a) and (c)] and $E = -J_0$ [(b) and (d)] eigenstates of the $\gamma = 0.3$ [(a) and (b)] and $\gamma = \ln(3)$ [(c) and (d)] lattices. The rest of the eigenstates are translations of the ones presented by an even number of sites. Red circles and red solid lines show numerical results. Blue circles and blue dotted lines correspond to the DS approximation in Eq. (B5). Green circles and green dashed lines correspond to the CF region approximation in Eq. (B11).

5. Numerically exact eigenstates and discussion

Figures 13 and 14 show results numerical results of a numerical diagonalization of the Hamiltonian in Eq. (B1) on a lattice with 201 sites $m = 0, \pm1, \pm2, \ldots, \pm100$ with Dirichlet boundary conditions. The parity of the coordinate of the leftmost site (i.e., the fact that -100 is an even number) effectuates the postselection condition that $m_{\mathrm{DS}} - m_{\mathrm{left}}$ must be even. This can be reformulated as follows: Our numerical procedure preserves only half of the eigenstates of the infinite lattice, namely those whose nodes in the $m \to -\infty$ region are located on the *odd* lattice sites.

We considered two values of the coupling decay rate γ: $\gamma = 0.3$ and $\gamma = \ln(3) \approx 1.10$. In the first case, coupling decay is slow enough to ensure the validity of the approximation in Eq. (B11). The second case corresponds to a lattice that is relevant to the problem in the main text. Figure 13 shows energy spectra in both the $\gamma = 0.3$ and $\gamma = \ln(3)$ cases. We noticed that in both cases, values $E = +J_0$ and $E = -J_0$ belong to the spectrum. We were not able to support this observation with an analytic result.

Next, we used the states $E = +J_0$ and $E = -J_0$ as a reference to verify the predictions in Eqs. (B7) and (B8). In both cases, the agreement between the numerical results and Eqs. (B7) and (B8) is remarkable. We also confirmed the prediction that the spectrum is symmetric with respect to the $+E \leftrightarrow -E$ transformation in Eq. (B6). Figure 14 shows the $E = +J_0$ and $E = -J_0$ eigenstates for both values of γ considered here. Both the DS [Eq. (B5)] and the CF region [Eq. (B11)] approximations work remarkably well. The validity of the approximation in Eq. (B11) for the $\gamma = \ln(3)$ case was unexpected, given the validity condition in Eq. (B12).

APPENDIX C: A CONJECTURE THAT THERE EXISTS AN INFINITE NUMBER OF EVEN NUMBERS WHOSE GOLDBACH DECOMPOSITION DOES NOT INVOLVE LOWER TWIN PRIMES

In this section, we conjecture that there is an infinite number of even numbers w that feature the no lower twin (NLT) property, i.e., that for any of the Goldbach decompositions of w, $w = p_1 + p_2$, both $p_1 + 2$ and $p_2 + 2$ are composite numbers. Note that unlike in the main text, here we do *not* assume that p_1 and p_2 are in any particular order with respect to each other.

In preparation, let us reiterate a well-known result that there do not exist triplets of consecutive (separated by 2) primes unless the lower member of the triplet is 3. We will need, however, a stronger version of this statement expressed in the following Lemma.

Lemma C1. Any lower twin prime p greater than 3 the following is true:

$$p \equiv 2 \pmod 3$$

Proof. First, since p is a prime different from 3,

$$p \equiv 1 \text{ or } 2 \pmod 3.$$

Second, since $p+2$ is also a prime different from 3,

$$p \equiv 2 \text{ or } 0 \pmod 3.$$

Combining the two we get

$$p \equiv 2 \pmod 3.$$ ■

We will also need to assert that

Lemma C2. All the even values of w such that

$$\text{(a) } w-3 \neq \text{prime}$$

$$\text{(b) } w \equiv 2 \pmod 6$$

possess the NLT property.

For example:

$$38 = 6\times 6 + 2 = 2 \mod 6$$
$$38 - 3 = 35 = 5\times 7 \neq \text{prime}$$
$$38 = 7 + 31 = 19 + 19$$
$$7 + 2 = 9 = 3\times 3 \neq \text{prime}$$
$$31 + 2 = 33 = 3\times 11 \neq \text{prime}$$
$$19 + 2 = 21 = 3\times 7 \neq \text{prime}.$$

Proof. Consider a Goldbach partition of w,

$$w = p_1 + p_2.$$

From the premise (a) it follows that

$$p_1 \neq 3$$
$$p_2 \neq 3. \tag{C1}$$

This can be proven using *reductio ad absurdum*. Assume that $p_2 = 3$. Then $p_1 = w - p_2 = (w-3) + (3-p_2)$ is a composite number, in contradiction to the premise that p_1 was a prime number. The assertion that $p_1 \neq 3$ can be proven analogously.

Next, it will follow from the premise (b) that

$$w \equiv 2 \pmod 3. \tag{C2}$$

We will utilize the statement in Eq. (C2), Lemma C1 to build a proof *ad absurdum*. Assume that p_1 is a lower twin different from 3. Then

$$p_2 = w - p_1 \equiv 2 - 2 \pmod 3 \equiv 0 \pmod 3.$$

However, this statement contradicts the premise that p_2 is prime different from 3. ■

We are finally ready to the principal theorem of this section:

Theorem C3. The number of even numbers possessing the NLT property is infinite.

Proof. Consider a sequence

$$w_k \equiv 2(15k+4)$$
$$k = 1,\ 2,\ 3,\ 4,\ \ldots. \tag{C3}$$

Let us first show that every member of this sequence obeys the premise (a) of the Lemma C2. Indeed,

$$2(15k+4) - 3 = 5(6k+1)\ ;$$

the right-hand side is a manifestly composite number unless $k = 0$ For the premise (b), we get

$$2(15k+4) = 6k' + 2,$$

with $k' = 5k+1$. ■

A comment is in order. The members of the infinite sequence (C3) used to prove the Theorem C3, may turn out to be a small subset of the full set of evens possessing the NLT property. Let us attempt to make an estimate of the density of evens in the former set. According to the prime number theorem, the number of primes below a number N is, approximately, $\pi(N) \approx N/\ln(N)$ [13]. It will immediately follow that for a given prime p_j, the next prime p_{j+1} will be separated from p_j by a gap—filled by the composite numbers—whose size is approximately $\ln(N)$. (Here and below, $p_1,\ p_2,\ p_3,\ \ldots = 2,\ 3,\ 5$ is the contiguous sequence of prime numbers in ascending order.) It will also follow that $p_j \approx j\ln(j)$.

The probability that a given number N obeys the premise (b) of Lemma C2 is $1/6$. The probability that a number of this type obeys the premise (a) is $1 - 2/\ln(N)$. Here $1/\ln(N)$ is the inverse of the gap between consecutive primes; the factor of 2 accounts for the fact that premise (b) implies that N is even and hence that $N-3$ is odd. Now, according to Lemma C2, the probability that a given number N is an even number that possesses the NLT property is $(1/6)(1-2/\ln(N)) \overset{N\gg 1}{\approx} 1/6$. All in all, we estimate that number of the even numbers obeying the NLT property that are less than N is

$$\pi_{\text{NLT, estimated}}(N) \overset{N\gg 1}{\approx} \frac{N}{6}. \tag{C4}$$

Interestingly, the rigorously justified subsequence (C3) properly captures the uniformity of the distribution estimated by Eq. (C4) but underestimates the density of the NLT even numbers by a factor of 5:

$$\pi_{\text{NLT, proven}}(N) \geqslant \frac{N}{30} - \frac{19}{15}. \tag{C5}$$

[1] G. Gauthier, T. A. Bell, A. B. Stilgoe, M. Baker, H. Rubinsztein-Dunlop, and T. W. Neely, *Dynamic High-Resolution Optical Trapping of Ultracold Atoms* (Academic Press, San Diego, CA, 2021), pp. 1–101.

[2] T. Harte, G. D. Bruce, J. Keeling, and D. Cassettari, Conjugate gradient minimisation approach to generating holographic traps for ultracold atoms, Opt. Express **22**, 26548 (2014).

[3] P. Zupancic, P. M. Preiss, R. Ma, A. Lukin, M. E. Tai, M. Rispoli, R. Islam, and M. Greiner, Ultra-precise holographic beam shaping for microscopic quantum control, Opt. Express **24**, 13881 (2016).

[4] J. yoon Choi, S. Hild, J. Zeiher, P. Schauß, A. Rubio-Abadal, T. Yefsah, V. Khemani, D. A. Huse, I. Bloch, and C. Gross, Exploring the many-body localization transition in two dimensions, Science **352**, 1547 (2016).

[5] K. Henderson, C. Ryu, C. MacCormick, and M. G. Boshier, Experimental demonstration of painting arbitrary and dynamic potentials for Bose–Einstein condensates, New J. Phys. **11**, 043030 (2009).

[6] G. Mussardo, The quantum mechanical potential for the prime numbers, arXiv:cond-mat/9712010.

[7] D. Schumayer and D. A. W. Hutchinson, Physics of the Riemann hypothesis, Rev. Mod. Phys. **83**, 307 (2011).

[8] M. Wolf, Will a physicist prove the Riemann hypothesis? Rep. Prog. Phys. **83**, 036001 (2020).

[9] D. Cassettari, G. Mussardo, and A. Trombettoni, Holographic realization of the prime number quantum potential, PNAS Nexus **2**, pgac279 (2023).

[10] F. Gleisberg, F. D. Pumpo, G. Wolff, and W. P. Schleich, Prime factorization of arbitrary integers with a logarithmic energy spectrum, J. Phys. B: At. Mol. Opt. Phys. **51**, 035009 (2018).

[11] G. Mussardo and A. Trombettoni, Integer factorization by quantum measurements, arXiv:2309.10757.

[12] F. Gleisberg, M. Volpp, and W. P. Schleich, Factorization with a logarithmic energy spectrum of a two-dimensional potential, Phys. Lett. A **379**, 2556 (2015).

[13] U. Dudley, *Elementary Number Theory* (W. H. Freeman and Company, San Francisco, 1969).

[14] C. J. Foot, *Atomic Physics* (Oxford University Press, Oxford, 2004).

[15] F. Bloch and A. Siegert, Magnetic resonance for nonrotating fields, Phys. Rev. **57**, 522 (1940).

[16] W. S. Bakr, J. I. Gillen, A. Peng, S. Fölling, and M. Greiner, A quantum gas microscope for detecting single atoms in a Hubbard-regime optical lattice, Nature (London) **462**, 74 (2009).

[17] C. Weitenberg, M. Endres, J. F. Sherson, M. Cheneau, P. Schauß, T. Fukuhara, I. Bloch, and S. Kuhr, Single-spin addressing in an atomic Mott insulator, Nature (London) **471**, 319 (2011).

[18] J. Sørensen, J. Jensen, T. Heinzel, and J. Sherson, QEngine: A C++ library for quantum optimal control of ultracold atoms, Comput. Phys. Commun. **243**, 135 (2019).

[19] N. Khaneja, T. Reiss, C. Kehlet, T. Schulte-Herbrüggen, and S. J. Glaser, Optimal control of coupled spin dynamics: Design of NMR pulse sequences by gradient ascent algorithms, J. Magn. Reson. **172**, 296 (2005).

[20] G. von Winckel and A. Borzì, Computational techniques for a quantum control problem with H1-cost, Inverse Probl. **24**, 034007 (2008).

[21] J. J. W. H. Sørensen, M. O. Aranburu, T. Heinzel, and J. F. Sherson, Quantum optimal control in a chopped basis: Applications in control of Bose-Einstein condensates, Phys. Rev. A **98**, 022119 (2018).

[22] O. V. Marchukov and M. Olshanii, Resonance cascades and number theory, AVS Quantum Sci. **7**, 013801 (2025).

[23] We exclude $0^2 + 0^2 = 0$ for technical reasons.

[24] L. Landau and E. Lifshitz, *Mechanics: Volume 1 (Course of Theoretical Physics Series)* (Butterworth-Heinemann, Amsterdam, 1976).

[25] S. E. Harris, Electromagnetically induced transparency with matched pulses, Phys. Rev. Lett. **70**, 552 (1993).

[26] E. Arimondo, Coherent population trapping in laser spectroscopy, Prog. Opt. **35**, 257 (1996).

[27] Interestingly, we find that any boundary condition at low m would instantly favor the sites of one parity over another; in the convention used, it is indeed always the odd sites that remain unpopulated in the low m tail of the eigenstates.

[28] Additionally, we verify that the observed drop in the cascade population is predominantly due to excitation to the continuum: The bound states outside the cascade remain unpopulated, thus verifying the resonant model.

[29] To the contrary, the sums of three squares are not closed under multiplication, e.g. $11 \times 373 = (1^2 + 1^2 + 3^2) \times (2^2 + 12^2 + 15^2) = 4103 \neq a^2 + b^2 + c^2$. Also, according to Lagrange's four-square theorem [13] (p. 146), the set of integers that are equal to the sums of four squares coincides with the set of all natural numbers.

[30] A relevant fact: If a is an integer that is equal to the sum of two squares, then the prime decomposition of a cannot contain a factor p^k such that p is a prime of the form $4 \times n + 3$, where n is an integer and k is odd.

[31] T. Caneva, T. Calarco, and S. Montangero, Chopped random-basis quantum optimization, Phys. Rev. A **84**, 022326 (2011).

[32] S. van Frank, M. Bonneau, J. Schmiedmayer, S. Hild, C. Gross, M. Cheneau, I. Bloch, T. Pichler, A. Negretti, T. Calarco, and S. Montangero, Optimal control of complex atomic quantum systems, Sci. Rep. **6**, 34187 (2016).

[33] C. A. Weidner and D. Z. Anderson, Experimental demonstration of shaken-lattice interferometry, Phys. Rev. Lett. **120**, 263201 (2018).

[34] A. Omran, H. Levine, A. Keesling, G. Semeghini, T. T. Wang, S. Ebadi, H. Bernien, A. S. Zibrov, H. Pichler, S. Choi, J. Cui, M. Rossignolo, P. Rembold, S. Montangero, T. Calarco, M. Endres, M. Greiner, V. Vuletić, and M. D. Lukin, Generation and manipulation of Schrödinger cat states in Rydberg atom arrays, Science **365**, 570 (2019).

[35] M. M. Müller, R. S. Said, F. Jelezko, T. Calarco, and S. Montangero, One decade of quantum optimal control in the chopped random basis, Rep. Prog. Phys. **85**, 076001 (2022).

[36] P. Parajuli, A. Govindarajan, and L. Tian, State preparation in a Jaynes-Cummings lattice with quantum optimal control, Sci. Rep. **13**, 19924 (2023).

[37] http://www.bris.ac.uk/acrc/.

[38] L. D. Landau and E. Lifshitz, *Mechanics: v. 1 (Course of Theoretical Physics)* (Butterworth-Heinemann, Oxford, 2000).

[39] L. D. Landau and E. Lifshitz, *Quantum Mechanics, Non-relativistic Theory: v. 3 (Course of Theoretical Physics)* (Pergamon Press, Oxford, 1977), chap . VII.

[40] L. D. Landau and E. Lifshitz, *Quantum Mechanics, Non-relativistic Theory: v. 6 (Course of Theoretical Physics)* (Pergamon Press, Oxford, 1977).

[41] M. Olshanii, *Back-of-the-envelope Quantum Mechanics: With Extensions to Many-body Systems and Integrable PDEs* (World Scientific, Singapore, 2013).

[42] N. Bleistein and R. Handelsman, *Asymptotic Expansions of Integrals* (Dover, New York, 1986).

[43] R. Mack, J. P. Dahl, H. Moya-Cessa, W. T. Strunz, R. Walser, and W. P. Schleich, Riemann ζ function from wave-packet dynamics, Phys. Rev. A **82**, 032119 (2010).

[44] M. V. Berry and K. E. Mount, Semiclassical approximations in wave mechanics, Rep. Prog. Phys. **35**, 315 (1972).